Icarus 359 (2021) 114343

Contents lists available at ScienceDirect

Icarus

journal homepage: www.elsevier.com/locate/icarus

Compositional control on impact crater formation on mid-sized planetary bodies: Dawn at Ceres and Vesta, Cassini at Saturn

P. Schenk [a,*], J. Castillo-Rogez [b], K.A. Otto [c], S. Marchi [d], D. O'Brien [e], M. Bland [f], K. Hughson [g], B. Schmidt [g], J. Scully [b], D. Buczkowski [h], K. Krohn [c], T. Hoogenboom [a], G. Kramer [e], V. Bray [i], A. Neesemann [j], H. Hiesinger [k], T. Platz [e], M.C. De Sanctis [l], S. Schroeder [c], L. Le Corre [e], L. McFadden [m], M. Sykes [e], C. Raymond [b], C.T. Russell [n]

[a] Lunar and Planetary Institute, Houston, TX, USA
[b] Jet Propulsion Laboratory, California Institute of Technology, Pasadena, CA, USA
[c] German Aerospace Center (DLR), Institute of Planetary Research, Berlin, Germany
[d] Southwest Research Institute, Boulder, CO, USA
[e] Planetary Science Institute, Tucson, AZ, USA
[f] Astrogeology Science Center, U.S. Geological Survey, Flagstaff, AZ, USA
[g] Georgia Institute of Technology, Georgia
[h] Johns Hopkins University, Applied Physics Laboratory, Laurel, MD, USA
[i] University of Arizona, Tucson, USA
[j] Freie Universitat Berlin, Berlin, Germany
[k] Westfälische Wilhelms-Universität Münster, Germany
[l] Istituto di Astrofisica e Planetologia Spaziali, INAF, Rome, Italy
[m] Goddard Space Flight Center, Greenbelt, MD, USA
[n] UCLA, Los Angeles, CA, USA

A B S T R A C T

High-resolution mapping of Ceres, Vesta and the icy satellites of Saturn, Uranus and Pluto reveals a rich variety of well-preserved impact crater morphologies on these low gravity bodies. These objects provide a natural laboratory to study effects of composition on crater formation processes under similar surface gravity conditions (though mean impact velocities vary by several factors). Simple craters occur on all these bodies but subtle differences in morphology on Ceres and Vesta are recognized. Immature complex craters (with large floor mounds but not terraces or conical central peaks) occur on Vesta and while smaller than predicted are consistent with its silicate composition. Asymmetric simple craters (with incomplete scarp development) on all bodies are likely related to differential overburden stresses in the rim, and their occurrence is consistent with lower crustal strength on icy bodies including Ceres. Immature and mature complex craters exhibit increasing degrees of complexity, including spiral floor deformation patterns (related to failure in converging floor material), central peaks, and impact melt. Cerean crater morphologic types and simple-complex transition diameters are smaller than on Vesta but similar to those on icy satellites, indicating a much weaker rheology for Ceres' outer layers under impact conditions. These are consistent with geophysical indications of a low-density water ice and probably clathrate rich outer shell. Fluidized floor deposits (impact melt or melt-solid mixtures) are significant in craters >25 km across on Ceres but absent on Saturn satellites. Central pit craters are common on Ceres (at diameters of ~75 to 150 km consistent with gravity scaling from the larger Galilean satellites) but are absent on Saturnian satellites and Charon. The contrasting impact melt and central pit behaviors on Ceres and Saturn's moons is contrary to expectation given the higher impact velocities at Saturn but might be related to lower internal temperatures, or the higher fraction of non-ice material on Ceres. The correlation or scaling of transition diameters to surface gravity is near −0.65 rather than −1, perhaps due to increased porosity on lower gravity bodies. The fundamental similarity of crater morphologies on Ceres and icy satellites, however, indicates that the weaker rheology of water ice results in similar craters even if the non-(ice+clathrate) components are as high as ~30 vol%.

1. Introduction

Impact cratering can be considered a form of violent brute force sampling of planetary crusts, involving rapid fracturing, melting, and mass movement within a large zone beneath a crater. As a result, the final form of such craters is modulated by bulk properties of crustal materials under very high strain rates. Planetary impact crater morphologies on terrestrial planets and the larger moons of Jupiter have

* Corresponding author.
E-mail address: schenk@lpi.usra.edu (P. Schenk).

https://doi.org/10.1016/j.icarus.2021.114343
Received 23 November 2020; Received in revised form 20 January 2021; Accepted 20 January 2021
Available online 26 January 2021

been shown to be strongly influenced by both surface gravity and by the mechanical properties of the target material (Pike, 1980; Schenk et al., 2004; Schenk, 2002). Impact craters in icy satellites rich in water ice have been found to be both significantly shallower and have smaller transition diameters (to increasingly complex landforms; e.g., simple-to-complex) than on silicate-rich target bodies of comparable surface gravity (Schenk, 1991).

Recent missions to the asteroid belt and the Saturn and Pluto systems have produced a bounty of high-resolution global mapping, compositional and topographic data for intermediate or mid-sized planetary bodies of differing compositions. These include the largest asteroids and the mid-sized satellites of Saturn, Uranus, and Pluto, all of which are approximately spheroidal and between roughly 400 and 1500 km in diameter (Table 1), the next largest objects being the much larger Triton, Pluto and Europa. We neglect Enceladus here due to its extensive resurfacing, tectonic deformation and lack of complex or pristine craters.

Conveniently, Ceres, Vesta and the mid-sized Saturnian satellites all have similar surface gravities between 10 and 30 cm/s^2 (Table 1), factors of 5 to 10 lower than those of the large icy satellites Europa, Ganymede and Callisto. This similarity in surface gravity among targets with very different compositions sets up a natural laboratory in impact mechanics, with the icy satellites (of Saturn and Uranus) and Vesta as icy and silicate end-members, respectively, and the more mixed interior of Ceres as a possible transitional case. Finally, we have the ice-rich Centaurs and trans-Neptunian objects, of which only Pluto and Charon have been explored directly (Moore et al., 2016). Pluto is a larger body and has also undergone moderate degree of erosion; Charon on the other hand is very similar in size and density to the mid-sized icy satellites though it may have a great abundance of low-temperature ices such as ammonia and methane (Dumas et al., 2001; Grundy et al., 2016; Dalle Ore et al., 2018).

Table 1
Physical properties of mid-sized planetary bodies.

Body	Radius (km)	Density, kg/m3	g, m/s^2	Surface Temperature*, K	Mean Heliocentric Impact Velocity**, km/s
Vesta	262.7	3456 ± 35	0.25	85–270	4–5
Ceres	469.7	2162 ± 10	0.28	130–240	4–5
Mimas	198.2	1149 ± 7	0.064	64	30
Tethys	531.0	985 ± 3	0.164	86	21
Dione	561.4	1478 ± 3	0.232	87	19
Rhea	763.5	1237 ± 2	0.264	53–99	16
Iapetus	734.3	1088 ± 13	0.223	90–130	6
Phoebe	106.5	1638 ± 33	0.045	73	3
Miranda	235.8	1200 ± 160	0.08	60 (mean), 84 (max)	12.5
Ariel	578.9	1592 ± 150	0.27	60 (mean)	10
Umbriel	584.7	1390 ± 160	0.2	75 (mean), 85 (max)	9
Titania	788.4	1711 ± 50	0.38	60–89	7
Oberon	761.4	1630 ± 50	0.346	70–80	6
Charon	606.0	1702 ± 20	0.29	53	2
Ganymede	2634.1	1.936	1.428	70–152	20
Callisto	2410.3	1.834	1.235	80–165	15
Moon	1738.1	3.344	1.62	100–390	17.5

* Temperature provided is the surface range when available, mean value otherwise.

** Mean impact velocities from Zahnle et al. (2003) and Williams et al. (2014a).

As Dawn approached the dwarf planet Ceres in early 2015 it was anticipated that impact crater morphologies there would, all other things being equal, most resemble those observed by Voyager and Cassini on these mid-sized icy moons, if the outer shell of Ceres were ice-rich. One of the objectives of the Dawn mission was to determine the surface and interior composition of the large asteroids Vesta and Ceres through global geophysical, geochemical and morphologic mapping of the body (Russell et al., 2012, 2016). Vesta (Russell et al., 2012; De Sanctis et al., 2012) is a very "dry" basaltic body (Table 1); Ceres is distinct among the larger asteroids for its lower density of at 2.162 g/cm^3. Gravity-shape studies of Ceres indicate a mixed ice-non-ice composition for its outer layers with a density of ~1.25 g/cm3 (Ermakov et al., 2017) corresponding to ~80 vol% ice+clathrate, assuming low porosity. Despite this, water ice has been detected spectroscopically on the surface by Dawn at only a few very small locations (Combe et al., 2016; Combe et al., 2019; Raponi et al., 2018). The icy satellites have ice-to-non-ice ratios between ~30 and ~ 100%, depending on porosity and other factors, with Dione likely being at least partially differentiated with an ice-rich crust (Zannoni et al., 2020) and Tethys being essentially all ice. The internal states of Rhea and Iapetus are less clear but the similarities in crater morphology to those on ice-rich Dione and Tethys (White et al., 2013, 2017) suggest that their outer layers are at least rheologically dominated by ice (Castillo-Rogez et al., 2018).

Other primary variables (Table 1) in crater formation include surface/internal temperatures, which are significantly lower on the Saturnian and Uranian satellites than either Vesta or Ceres, and impact velocities, which are higher. Mean impact velocities are ~5 km/s for both Vesta and Ceres but may be as high as 30 km/s for heliocentric impactors in the inner Saturn system, or as low as ~2 km/s for the Kuiper Belt. Increasing impact velocity obviously increases crater size but likely also increase melt production (e.g., Pierazzo et al., 1997; Keil et al., 1997; Cintala and Grieve, 1998; Williams et al., 2014a). Planetocentric populations can also be important in the satellite systems (cf. Kirchoff et al., 2018). We do not address directly the issues of post-impact degradation or the role of porous targets, on the assumption that impact generated regolith porosities on these heavily cratered bodies are broadly similar, though observationally unconstrained.

1.1. Data and analysis

Various global mapping products are used to catalog and measure crater shapes and morphologies and compare the variability of major landforms on these distinct bodies. Dawn global image and topography mapping of Vesta down to resolutions of ~20 m GSD (ground sampling distance) and ~ 35 m GSD for Ceres (supplemented by very limited mapping at ~3.5 m GSD) were produced from Dawn imaging (Preusker et al., 2016; Park and Buccino, 2018; Roatsch et al., 2016). Global Cassini image and topography mapping of the Saturnian satellites at effective resolutions of 250 to 400 m (and to as good at ~30 m in a few locations) are now essentially complete for the 6 mid-sized Saturnian satellites (Schenk et al., 2018a). New Horizons image and topography mapping of Charon to as good as ~150 m GSD and in which crater morphologies can be ascertained has also been acquired for ~40% of its surface (Schenk et al., 2018b).

A key to our work is our survey and catalog of crater morphologies and dimensions of impact craters on Ceres and Vesta, including location, diameter, rim-to-floor depths where measurable, and floor morphologies (including but not limited to floor mounds, terraces, central peaks and pits, rim slides, melt-like deposits, and ejecta (though we do not address ejecta in this report)) as well as their dimensions. The simple-to-complex transition can be measured in several ways and is not abrupt but spread over a multiple kilometer range (Pike, 1980). This is in part because the formation of features such as terraces, floor deposits, central peaks and other structures in larger craters do not begin to appear at the same diameter and because local variations in target properties and

impact conditions (e.g., velocity and angle) result in variations in crater modification. Here we use the criteria for determining the morphologic transition from bowl-shaped simple craters to central peak craters of Pike (1980) based on a statistical measure of when central peak craters are >50% of the total craters in the size bins which were usually 5 km wide with comparable uncertainties, and the inflection in the depth-to-diameter (d/D) curve. In some cases, the number of pristine craters in larger size bins are <10, but we were able to accumulate enough statistics to define transition diameters in most cases. Depth/diameter transitions are based on the intercepts of the least-squares fits to data for simple and complex craters.

Because smaller scale central peaks, terraces, melt textures are the first to fade due to post-impact erosive forces, we consider here only those craters that are relatively pristine and whose original morphologies are well-preserved and can still be ascertained through imaging. Our preservation states are subjectively defined as 1, no or negligible superposed cratering, all structures and textures preserved; 2, light superposed cratering, most structures and textures preserved, some rounding of and partial loss of smallest-scale features; 3, moderate superposed cratering, loss of smaller-scale textures such as boulders and smaller ridges; 4, significant superposed cratering, loss of many structures and textures, though large-scale features such as large peaks, terraces and rim scarps preserved; 5, superposed crater density indistinguishable from background, loss of all structures and textures, rounding and degradation of crater rim. Our discussion here is restricted to those craters with preservation states 1 to 3, and 1 to 4 in craters larger than ~75 km due to the smaller number of such craters.

Preliminary findings for Ceres and Vesta crater morphologies have been published by Hiesinger et al. (2016) and by Schenk et al. (2016) and this report represents the completion of that work. An independent survey of thousands of Ceres' craters has been made by Zeilnhofer and Barlow (2020) but our catalog and analysis here considers only pristine craters in order to better understand primary landforms in an interplanetary comparative context in the absence of degradation effects. White et al. (2013, 2017) report on crater morphologies for the Saturnian satellites, which we summarize and augment here. Schenk (1989) reported crater morphology data for the Uranian satellites but the Cassini results of White et al. (2013, 2017) demonstrated that earlier Voyager topographic and morphometric data are unreliable for smaller craters <10 pixels across in imaging. In the Uranian system this leaves only heavily resurfaced Ariel and Miranda (where simple craters dominate), where a few fresh complex craters appear to be similar to saturnian satellites but not sufficiently to characterize morphologies globally. Schenk et al. (2018) and Robbins et al. (2020) report on crater morphology results for Charon. For Vesta, we also compare crater morphologies to lunar impact craters, as the Moon is the next largest "ice free" silicate body with complex crater morphologies (despite the factor of 5 higher surface gravity and higher mean impact velocities on the Moon; Table 1).

2. Crater morphologies on Vesta

We begin with a survey of fresh crater morphologies on Vesta, which represents an end-member in the ice-silicate compositional spectrum due to its extremely low (<1%) bulk crustal volatile composition (Sarafian et al., 2019). Vesta is the largest silicate-rich asteroid visited to date and the only one to exhibit complex crater morphologies. The giant Rheasilvia impact basin (Schenk et al., 2012) at 500-km-diameter is similar in radius to Vesta itself. In forming, Rheasilvia obliterated all of the original southern hemisphere and mantled with ejecta or degraded by seismic shaking most of the northern hemisphere of Vesta ~1–1.7 Ga ago (Schenk et al., 2012; Marchi et al., 2012; Yingst et al., 2014), thus erasing or heavily modifying the pre-basin cratering record across Vesta prior to that time. Though of unknown age, the formation of the overlapping older 400-km Veneneia basin near the south pole also contributed to this damage. While older large craters are observed in the northern hemisphere, only those in which original morphologies have not been blanketed or obscured by Rheasilvia effects are described and considered here, though this provides us with fewer large impacts to compare with Ceres or other bodies. The largest of these relatively well-preserved post-Rheasilvia impact craters is ~62-km-diameter Marcia.

2.1. Simple Craters on Vesta

With the exception of several larger transitional craters described in the next section, most post-Rheasilvia craters on Vesta are classified as simple craters: bowl-shaped depressions with little or no floor fill and no central peaks or terraces (although a few craters have limited rim slump blocks (e.g., Octavia). Smaller simple craters have rounded rubble-strewn rims while larger simple craters on Vesta have steep sharp-edged inner rim walls formed by mass wasting scarps (Fig. 1) giving them a rounded "V" shape. Many craters can exhibit both rim styles in different rim sections (Krohn et al., 2014b) and this contrasting rim morphology aspect is discussed in a planetary context in the Asymmetric Craters section below.

In the freshest simple craters, slump features in the form of very narrow down-slope deposits with lobate termini are resolved along most of the rim scarp (Fig. 2), forming a semi-continuous apron around the rim scarp. These downslope mass wasting deposits most likely form by instantaneous small landslides triggered during or just after impact (Otto et al., 2013; Krohn et al., 2014a). Long grooves parallel to slump margins are common within these rim wall debris aprons of simple craters on Vesta and have been interpreted as gullies, some formed by "dry" granular downslope flow, others by "wet" transient debris-flow-like processes, based on subtle differences in morphology (Scully et al., 2015). The "dry" gullies are medial septa formed between or within discrete flow lobes, probably formed as a result of differential flow velocity, and are similar to those observed on lunar simple craters (Fig. 3). Such adjacent longitudinal flow lobes are common within landslide deposits, consistent with the observation that the "dry" gullies greatly outnumber the "wet" gullies on Vesta. The "wet" gully hypothesis is currently being investigated via laboratory experiments and additional geomorphological analysis (Scully et al., 2020a), and we do not discuss these features in further detail here.

Debris mounds are usually not observed at the base of the crater rim walls or across crater floors (Figs. 1–3), indicating that mass wasting volumes of the rim slumps are not large enough to form more than surficial flows. In some cases we observe spatially limited flat-floor deposits of small area and low volume at crater bottom. The small volumes of floor materials even in the largest well-preserved craters on Vesta (D ~ 67 km) contrast sharply with the floors of most lunar craters larger than 15 km, which are filled with extensive flat-lying knobby or lobate floor deposits with pseudo-volcanic morphologies (Fig. 3). These are interpreted as impact debris+melt deposits that accumulated on the floor during the crater collapse and solidified and cooled in place. In the largest post-Rheasilvia crater, Marcia, localized smooth deposits resembling impact melt (Fig. 4g) are scattered within local topographic lows in the ejecta deposit and near the center of the crater (e.g., Williams et al., 2014a; Michalik et al., 2020) but do not appreciably fill the crater. In general, the apparent volume of impact melt ponded in the floors and ejecta of post-Rheasilvia craters is much less than on the Moon (Figs. 2, 3), consistent with predictions that melt volumes would be much lower (Marchi et al., 2013) due to the lower mean impact velocities on Vesta (Keil et al., 1997) compared to the Moon or Mercury.

In some of the youngest Vestan craters the limited floor deposits are pitted in a manner similar to Martian craters (Fig. 2; Denevi et al., 2012). The pits are inferred to be explosion or outgassing pits formed by volatile escape from within a (volumetrically small) solidifying impact melt deposit. The amount of vapor inferred to form such pits might plausibly be as high as 30 wt% of the melt (Michalik et al., 2020), though the pitted floors show a lower content of OH with respect the surrounding dark material, suggesting that part of the material containing OH is

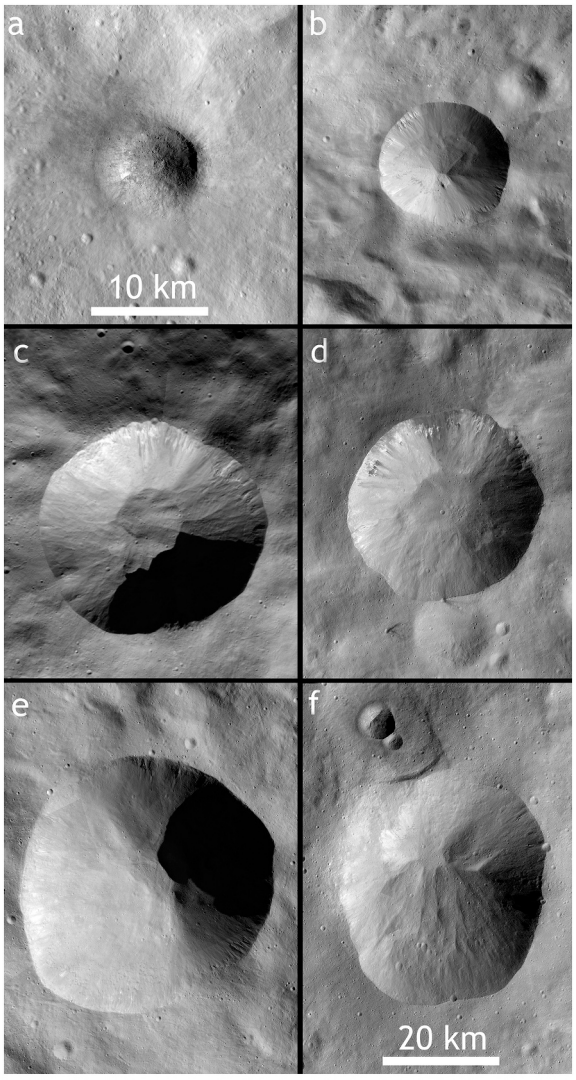

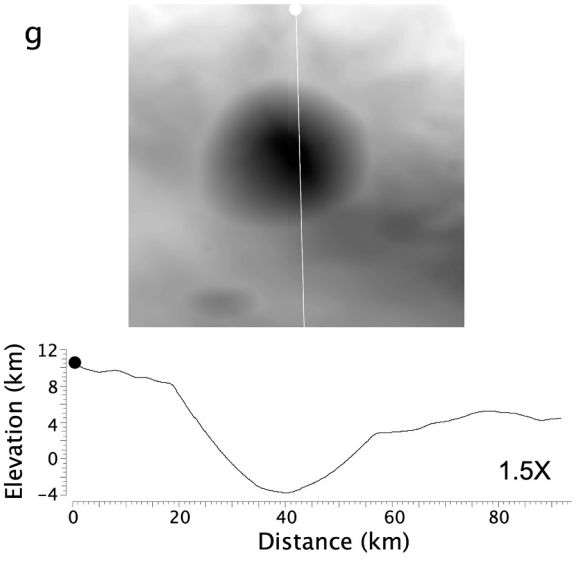

Fig. 1. (a–f). Simple craters on Vesta, with diagnostic steep continuous rim scarp and minor or negligible floor fill. Craters are (a) ~8 km, 28S, 225E; (b) D ~ 19 km (53S, 142E), (c) D ~ 35 km (49N, 292E), (d) Numisia, D ~ 30 km, (e) Tarpeia, D ~ 40 km, (f) Oppia, D ~ 35 km (note small simple craters to upper left). Smaller crater (a) has rounded rubble-strewn rim, all others rim scarps and slumping. All images to scale (20 km bar) except (a) which is enlarged 200% to show detail. North is to top in all figures unless noted. (g) Profile of Tarpeia crater. Inset map above profiles is from the global elevation model of Vesta (Preusker et al., 2016).

(caption on next column)

removed by the impact (De Sanctis et al., 2015). The mechanism of formation is not well defined but perhaps the pits form when gaseous volatiles are driven out through fissures from directly beneath the impact site by residual impact heat, forming collapse pits mainly in melt materials that have not yet completely solidified. Regardless of formation, HED samples and Vesta's bulk density confirm a very low water ice content for this body (Sarafian et al., 2019).

2.2. Immature complex craters on Vesta

Direct g^{-1} extrapolation of the simple-to-complex transition diameters for terrestrial bodies (either the d/D intercept or 50% occurrence of complex morphologies) predicts transition diameters for Vesta of ~80–100 km. Although no post-Rheasilvia craters >65 km are preserved, transitional morphologies are observed on Vesta. At least eight post-Rheasilvia transitional craters 35 to 65 km across have been identified to date (Fig. 4): Pinaria, Bellicia, Marcia, Drusilla (Fig. 2), Caparronia, and craters at 70N, 105E, 46N, 354E, and 73N, 52E (all Vesta longitudes are in the Claudia system). The 88-km degraded immature flat-floored crater at 73N, 51E is another example. These craters have distinctly non-circular simple rim scarps and large irregularly shaped floor mounds (Fig. 4), replacing the inverted conical bowl shapes of simple craters. They are also up to 20% shallower than simple craters of similar size, despite the fact that no appreciable flat-lying floor-fill deposits are evident even in these larger craters.

Similar transitional complex craters near the simple-to-complex transition diameter are common on the Moon (e.g., Dawes, D ~ 18 km, Fig. 5), featuring similar irregular shapes with hummocky floor morphologies and shallower depths than same-sized simple craters (Cintala et al., 1977; Pike, 1980; Clayton et al., 2013). These craters lack the coherent structural terrace blocks or central peaks of larger complex craters on the Moon and are regarded as transitional to fully developed complex craters (Cintala et al., 1977). They likely represent the initial stages of crater collapse and we follow the Pike (1980) "immature complex crater" taxonomy for these craters.

The 67-km crater Marcia (Fig. 4) features an arcuate elevated plateau within a deep rim reentrant along the southern rim, indicative of partial rim failure, as well as several small floor mounds at crater center (Williams et al., 2014a, 2014b). The floor mounds are <1 km high and do not form a classic conical central peak. Marcia's floor mounds are thus regarded as possible nascent central peaks in a crater too small on Vesta to develop larger classic conical central uplifts of the type seen on other planets or in the much larger Rheasilvia below. If Vestan craters possessed larger volumes of debris and impact melt deposits these small mounds would have been buried. These features place Marcia in the immature complex crater class and indicate the transition to central peaks on Vesta occurs at greater than 65 km.

2.3. Mature complex craters on Vesta (i.e., Rheasilvia)

The only fully developed and well-preserved complex crater on Vesta is the 500-km-diameter Rheasilvia basin (Fig. 6; Schenk et al., 2012). (The 400-km-wide Veneneia basin truncated by Rheasilvia is too disrupted to retain its original landform type and its central region is essentially coincident with the overprinted Rheasilvia rim.) Rheasilvia in outline features a deep bowl-shaped crater floor surrounding a

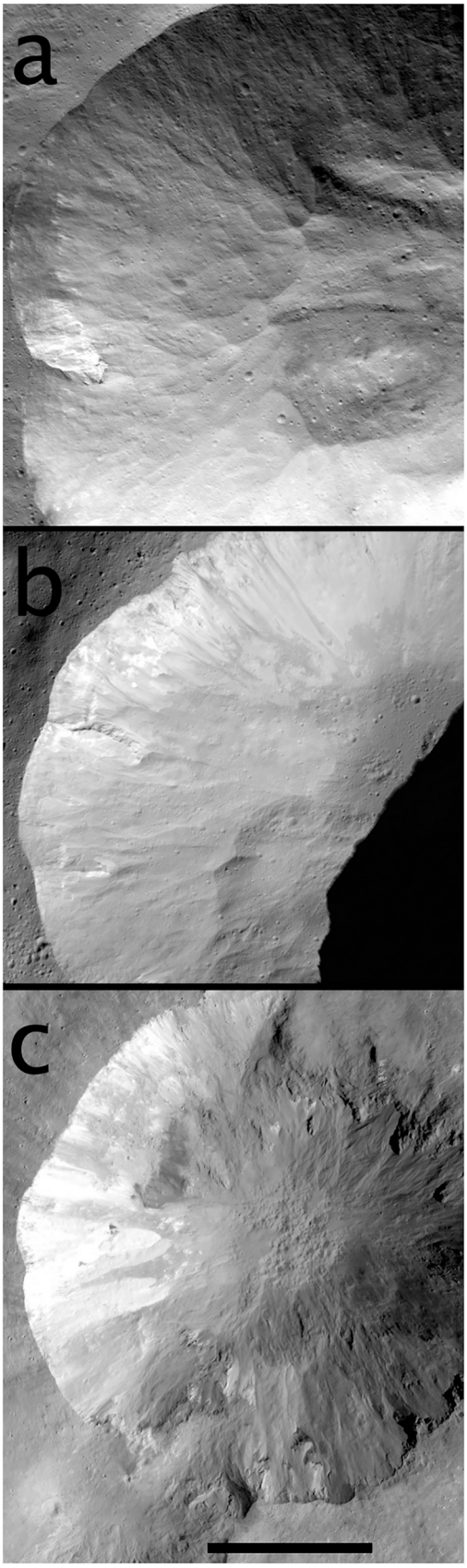

Fig. 2. Enlarged views of finger-like and lobate rim wall slump deposits in Vesta craters. (a) Drusilla, ~21 km; (b) Licinia, ~23 km; (c) Cornelia, ~15 km. Scale bar is 5 km.

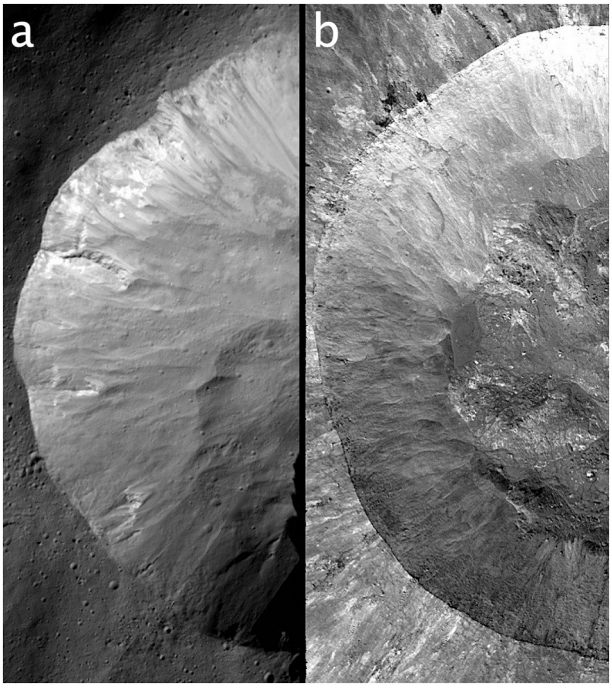

Fig. 3. Dawn and LROC images of fresh craters on Vesta (a, Licinia, 24 km) and the Moon (b, Giordano Bruno, 22 km). Images to scale. Note similarity of multiple contiguous narrow rim slides, and presence of large amounts of accumulated debris and melt on the floor of G. Bruno. Note that with inverse gravity scaling, G. Bruno is equivalent to ~35 km craters on Vesta, which also lack significant volumes of accumulated impact melt.

prominent 22-km-high 150-km-wide central peak. As with the immature complex craters on Vesta, flat-lying floor fill deposits are lacking, resulting in a rounded "W" crater shape (after removal of planetary curvature). Although difficult to measure precisely due to the fact that the original surface of the south polar terrains is unknown, a depth of ~20 ± 5 km was estimated from a best fit to the existing non-Rheasilvia surface. The basic shape and morphology is broadly similar to large central peak impact basins on Iapetus, Hyperion and Rhea (Schenk et al., 2012), suggesting that this general morphology is typical of larger impacts into smaller lower gravity bodies.

The Rheasilvia central peak has a craggy mountainous appearance indicative of disrupted basement rock and consistent with uplift of floor material during impact. The floor is relatively smooth on sub-kilometer scales but is cut by numerous parallel curvilinear scarps and undulating ridges which form a distinctive clockwise radial-to-spiral pattern. These patterns are consistent with Coriolis deflection due to the rapid rotation (~5 h) (Schenk et al., 2012; Otto et al., 2016) of the floor material as it moved toward basin center during floor uplift and rim subsidence during the immediate crater modification stage. These floor features also have important implications for the age of the impact event at Rheasilvia, which are discussed in a companion paper (Schenk et al., 2020b).

2.4. Crater depths and the simple-complex transition on Vesta

Vincent et al. (2014) measured shapes of several hundred craters on Vesta, reporting for example d/D ratios of simple craters on the younger surface of Rheasilvia of ~0.19. They include craters in a range of degradation states which have reduced their apparent depths. We limited our survey to only the least degraded crater states in order to characterize the shapes of intact craters. The pervasively undulating relief of Vesta (Preusker et al., 2016) makes it difficult to determine original local reference planes, limiting the number of fresh craters for which we currently have robust relief data. Nonetheless, those pristine

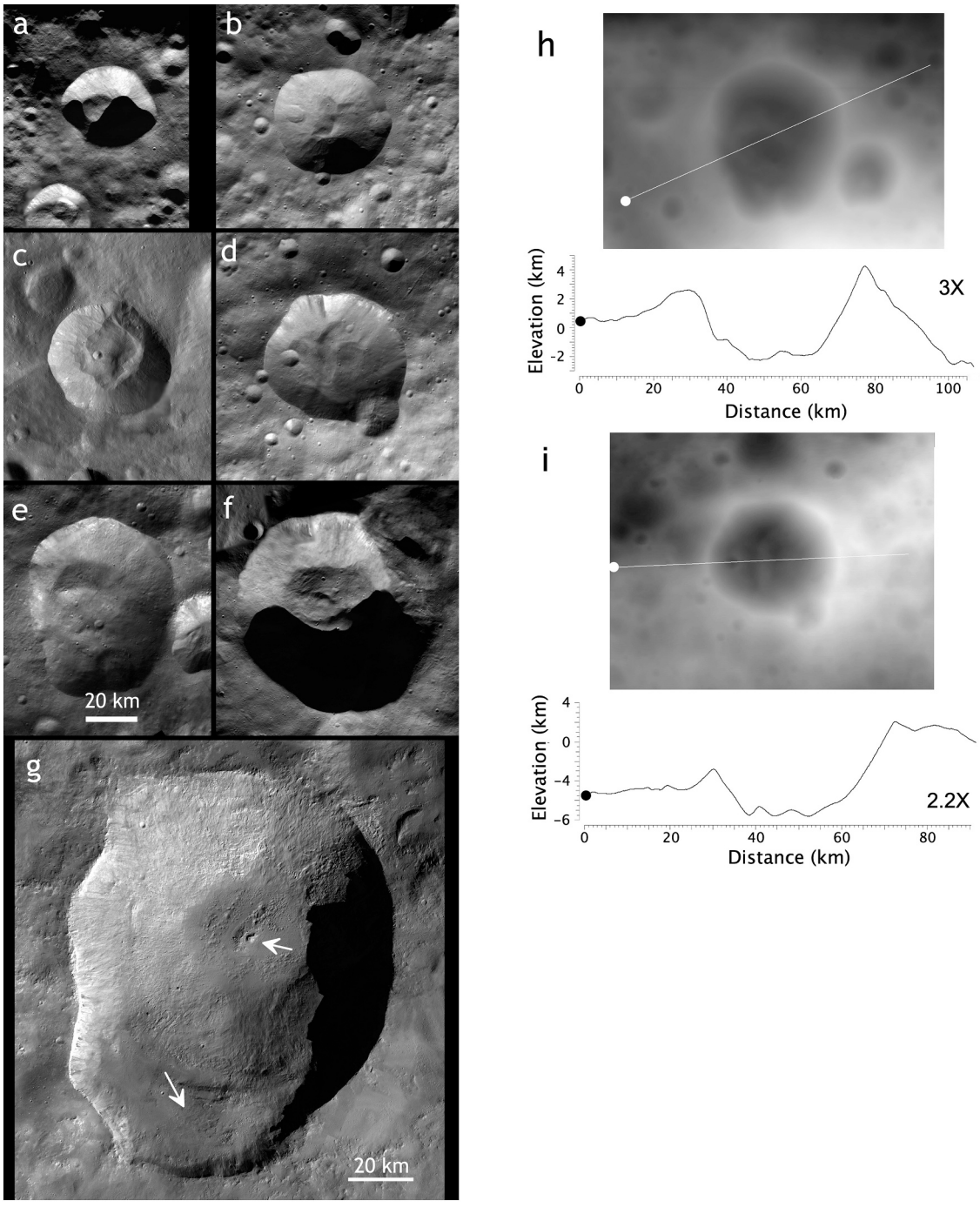

Fig. 4. (a–g). Immature complex craters on Vesta. From top left: (a) ~25 km (69N, 195E); (b) ~34 km (46N, 354E); (c) Pinaria, ~39 km; (d) Bellicia, ~42 km; (e) Caparroni, ~49 km; (f) ~60 km (70N, 113E); (g) Marcia, ~67 km, large bench on southern rim and very small central hills indicated by arrows. Scale bar for a–f is 20 km. Images to scale except Marcia. (h), i. Profiles of immature complex craters Bellicia (h), ~42 km and Caparroni (i), ~49 km. Top insets are excerpted from global DEM (Preusker et al., 2016).

simple craters for which such data has been obtained have rim-to-floor depth-diameter ratios of ~0.22 (Fig. 7), slightly higher than canonical lunar craters (e.g., Pike, 1980) and the mean value of Vincent et al. (2014). Even fewer rim height measurements (relative to ground plane) were possible (without more sophisticated slope analyses). For the few cases that can be reliably measured, rim heights are systematically higher than on the Moon by factors of 2 to 3 (Fig. 7). These observations suggest that either ejecta deposits are thicker on Vesta, rim uplift during excavation is greater (presumably due to the lower gravity), or (based on the much more limited rim scarp mass wasting) rim collapse is less extensive than on the Moon, resulting in less diameter enlargement and more preservation of the original transient cavity rim structure which would also have the effect of preserving the thicker and higher inner parts of the ejecta deposit.

Although we see only one well-preserved crater large enough on Vesta to produce true complex landforms (Rheasilvia), leaving a large gap between 65 and 500 km, we infer that we are seeing the transition to complex morphologies on Vesta in the form of the immature complex craters between ~30 and 65 km. These craters on Vesta (Fig. 5) have d/D ratios shallower than the 0.2–0.25 typical of simple craters on Vesta

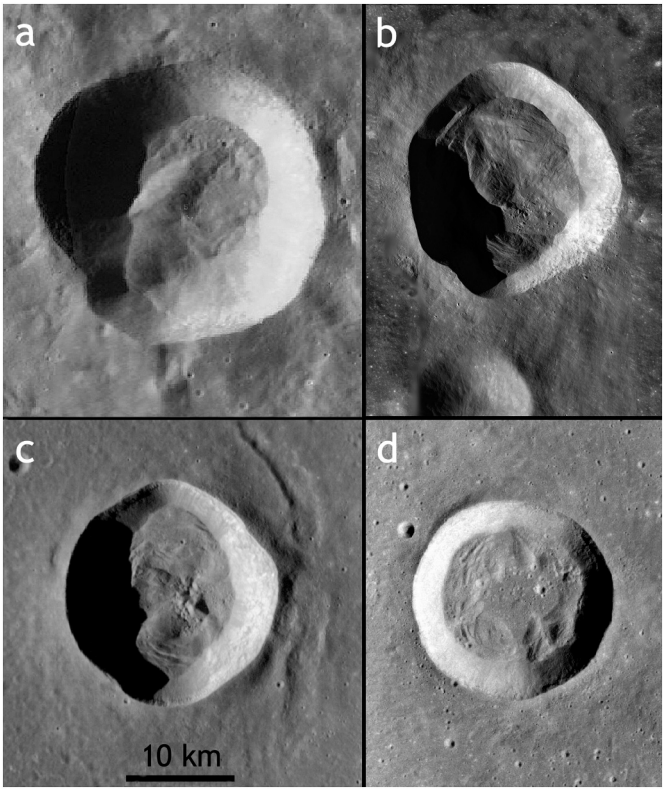

Fig. 5. Immature complex craters on the Moon with extensive mounded floor deposits. From top left, (a) Koval'skiy P, 25 km; (b) Larmor Q, 22 km; (c) Dawes, 18 km; (d) Bessel, 16-km. Compare to Fig. 4. All craters shown to same scale.

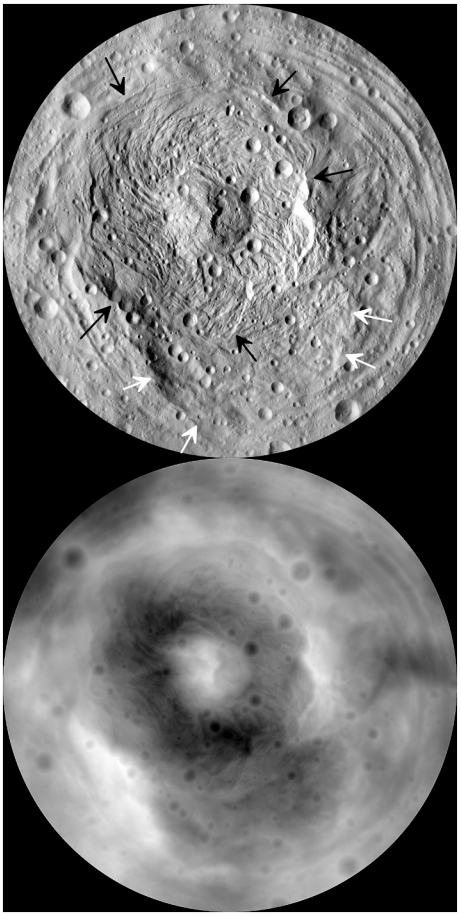

Fig. 6. Southern hemisphere projection of Vesta showing 500-km Rheasilvia impact basin. Top is shaded relief map; bottom is topographic map from global DEM (Preusker et al., 2016), with 20 km of relief shown. Large circular massif just left of center is the 10-km-high central peak, with rim scarp highlighted by black arrows. Preserved half of Veneneia basin is visible outside Rheasilvia rim (white arrows), toward bottom of view. Moderate superposed cratering is evident throughout, including basin floor and ejecta.

(Fig. 7) and form a d/D trend line with a shallower non-proportional slope of ~0.34. The intercept of the least-squares fit for these immature complex craters with the measured simple craters gives a nominal d/D simple-to-complex transition diameter of ~29 km (±3 km) for Vesta (Fig. 7), roughly consistent with our observed morphologic transition to immature complex morphologies of 35 ± 5 km. These values are similar to but updated from Vincent et al. (2014) using our catalog of pristine craters. We note that the apparent depth/diameter of Rheasilvia plots on the extrapolation of immature complex crater d/D trend as do the depths of several larger degraded impact features that predate Rheasilvia and are recognized in the global topographic map (Fig. 7). The shallow d/D slope for immature complex craters is comparable to that of lunar complex craters (Fig. 7), and consistent with the conclusion that these craters form the lower segment of the complex crater d/D curve on Vesta.

3. Crater morphologies on mid-sized icy satellites

3.1. Simple craters on icy satellites

The icy moons of the outer planets represent the ice-rich end-members of the ice-silicate mid-sized compositional spectrum. Most smaller craters on icy satellites less than ~10 km across are "simple" bowl shaped depressions, with variable degrees of minor floor fill. High-resolution mapping coverage and topographic data (at <50 m/pixel) for small pristine simple craters on these bodies is very limited, and only a few are resolved sufficiently to identify primary features (Fig. 8). Simple craters on icy satellites feature a steep inner rim scarp and small area of hummocky deposits on the floor. Down-slope bright and dark streaks suggestive of rim sliding of debris are sometimes resolved. Although on the smallest and lowest gravity body in our survey (Table 1), resolved simple craters on Phoebe (Fig. 8) occur in both rounded rubble-strewn rim and sharp rim scarp styles (similar to Vesta), and lack significant flat-lying floor deposits. Rim scarps often have downslope streaks that may be similar to those at Vesta (Fig. 1). A peculiarity of many craters in the Saturnian system is that under high-solar illumination, rims scarps are relatively bright and often have a relatively bluish color (i.e., bright in green and UV filters; Fig. 8h). This has been attributed to the exposure of larger grains of ice on the steep rim scarp (Schenk et al., 2011; Schenk et al., 2018a). The 10-km simple crater on Dione in Fig. 8 features several curvilinear markings on the southern rim flank suggestive of deceleration dunes in an ejecta deposit (Fig. 8f), perhaps similar to those flanking several Vestan (Fig. 1) and lunar simple craters (e.g., Linne).

3.2. Immature complex craters on icy satellites

Complex craters are the dominant landform at diameters greater than approximately 10 km on all our mid-sized icy satellites. Smaller complex craters here are characterized by steep rim wall scarps with slopes of 30–40° transitioning abruptly to hummocky floor textures without coherent central peaks or concentric slump terrace blocks. These are also classified as immature complex craters (Fig. 9). These hummocky floor deposits cover more than ~33% of the apparent crater diameter, distinguishing them from the volumetrically minor rim slump materials accumulated at the bottoms of simple craters. The floor

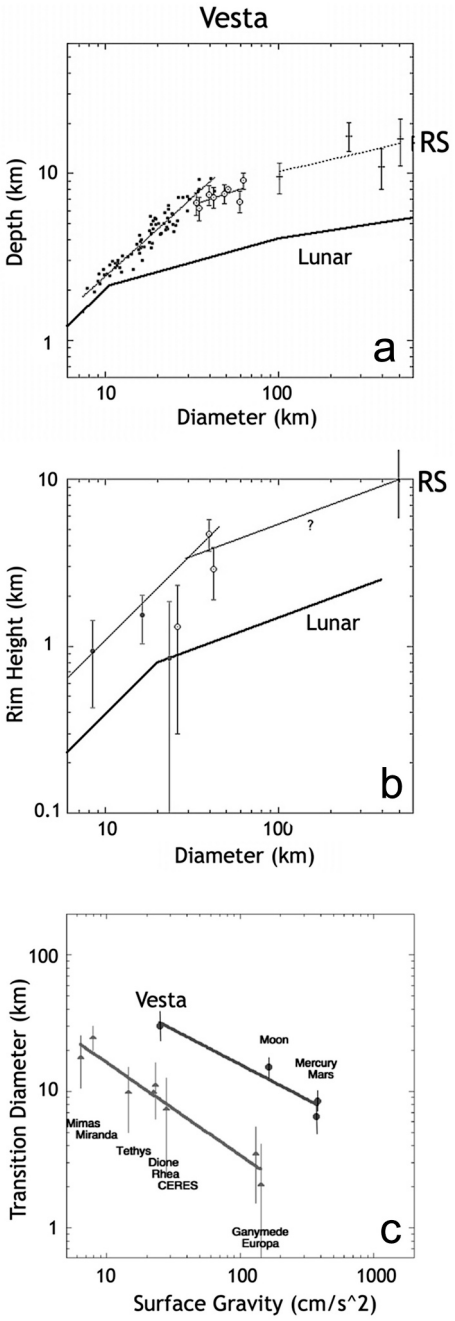

Fig. 7. Crater depths (a), rim heights (b), and transition diameters (c) for depth/diameter intercept on Vesta, the inner silicate-rich planets and icy satellites. The fits for the rim height data (thin lines, center plot) are nominal fits assuming slopes of the lunar data (Pike, 1980). RS is Rheasilvia.

structures in these craters (Fig. 9) are not flat-floored, such as at Copernicus or Tycho, but consist of rounded or scarp-bounded arcuate ridge and mound structures wreathed together to form disorganized patterns with uneven relief (Schenk et al., 2020a). Individual mounds, hummocks or ridges are no more than ~100 m high. Some of these craters can have a distinctly irregular shape with asymmetric floor deposits (Fig. 9f) due to rugged pre-impact relief. Many terrains on these moons are effectively saturated in craters (Fig. 9), and new impacts into these deeply pocked terrains will induce irregularities or asymmetries in crater excavation and collapse, wherein one side forms in terrains several kilometers above or below the rest of the crater, especially when the scale of topographic variability is comparable to that of newly formed craters.

3.3. Mature complex (central peak) craters on icy satellites

At larger crater diameters (>15–20 km), mature complex craters have rim and floor morphologies (including ridged floor units) similar to immature complex craters (Fig. 9) except for the emergence of recognizable central peaks and greater degrees of organization to the ridges and scarps of the floor deposits (Fig. 10). The floor ridges and scarps can often exhibit concentric or spiral patterns. Central peaks tend to increase in height and width as the crater diameter enlarges, and in craters larger than ~50 km central peaks are usually very prominent, forming roughly symmetric cones (Fig. 10a) up to 5 km high (nearly 10 km in basins larger than 500 km across). Peaks can be irregular or linear in shape within craters formed on rugged terrains.

The 49-km extremely young bright ray crater Inktomi on Rhea (Schenk et al., 2020a; Fig. 10f) is the best resolved fresh crater on the icy satellites. Inkomi was observed by Cassini in stereo and color at ~32 m/pixel (Schenk et al., 2020a), comparable to global mapping resolutions of Ceres (next sections). Inktomi is a typical central peak crater, with a steep single rim wall scarp, extensive undulating hummocky ridged floor unit and modest central peak. Several small and likely post-impact landslide units occur along the base of the rim wall scarp but these are volumetrically insignificant compared to the ridged floor unit. The 1-km-high central peak consists of a quasi-conical massif with several ridges extending outward. Although extensive ejecta mantling is observed, no evidence is observed for post-impact fracturing or accumulated or ponded impact melt on the floor or ejecta of this or in any other similar fresh large craters in the Saturn system (Figs. 9, 10; Schenk et al., 2020a).

Inktomi also features definitive secondary craters, as do several other craters of similar size (Schenk et al., 2020a). These are evident as fields of irregular-shaped and sharp-rimmed craters up to a few kilometers across approximately one crater diameter from the rim (Fig. 10f). Inktomi is also unusual for the dense field of small craters on the eastern floor and rim of this very young crater, interpreted as fallback of self-secondaries onto the floor (Schenk et al., 2020a). Although we do not discuss ejecta and secondaries here, we note their occurrence on these satellites.

Similar complex craters are observed on Charon, with steep rim scarps, hummocky and ridged floor deposits, ejecta facies, and conical to elongate central peaks of various shapes in the larger complex craters (Fig. 11). Because the best Charon images are 155-to-300 m GSD, more detailed comparisons are not possible but, to our ability to resolve, these craters resemble those observed on Saturnian icy satellites (Schenk et al. 2018; Robbins et al., 2020), despite the low surface temperatures of ~35 K and the possibility of significant ammonia in Charon's crust (Dalle Ore et al., 2018).

3.4. Mature complex (central pit) craters on icy satellites

On Ganymede and Callisto (Schenk, 1991; Schenk et al., 2004) central pits (small depressions) replace central peaks in craters >30 km. Pits on Ganymede are typically not more than 1 km deep, and in craters greater than ~60 km across, pits are partially filled by a rounded dome up to 1.5 km high (Schenk, 1993). Two candidate central pit craters (82-km at 6°S, 155°E and 46-km at 10°N, 155°E) occur on Pluto (though both are located in ancient ridge-trough system) but none have been recognized on Charon (Robbins et al., 2020) or in the Saturnian and Uranian systems (Schenk, 1989). Inverse gravity scaling of central pit crater occurrences on Ganymede and Callisto predicted this transition should occur at ~60–150 km diameters on the mid-sized Saturnian satellites and on Ceres (Schenk et al., 2019). Instead, even the largest impact structures observed (~350 km on Dione and ~ 750 km on Rhea and Iapetus) are characterized by large conical central peaks dominating ~1/3rd the crater floor (White et al., 2013, 2017). The lone exception to the dominance of central peaks at the largest basin diameters is 400-km-diameter basin Odysseus on Tethys, which most resembles the central

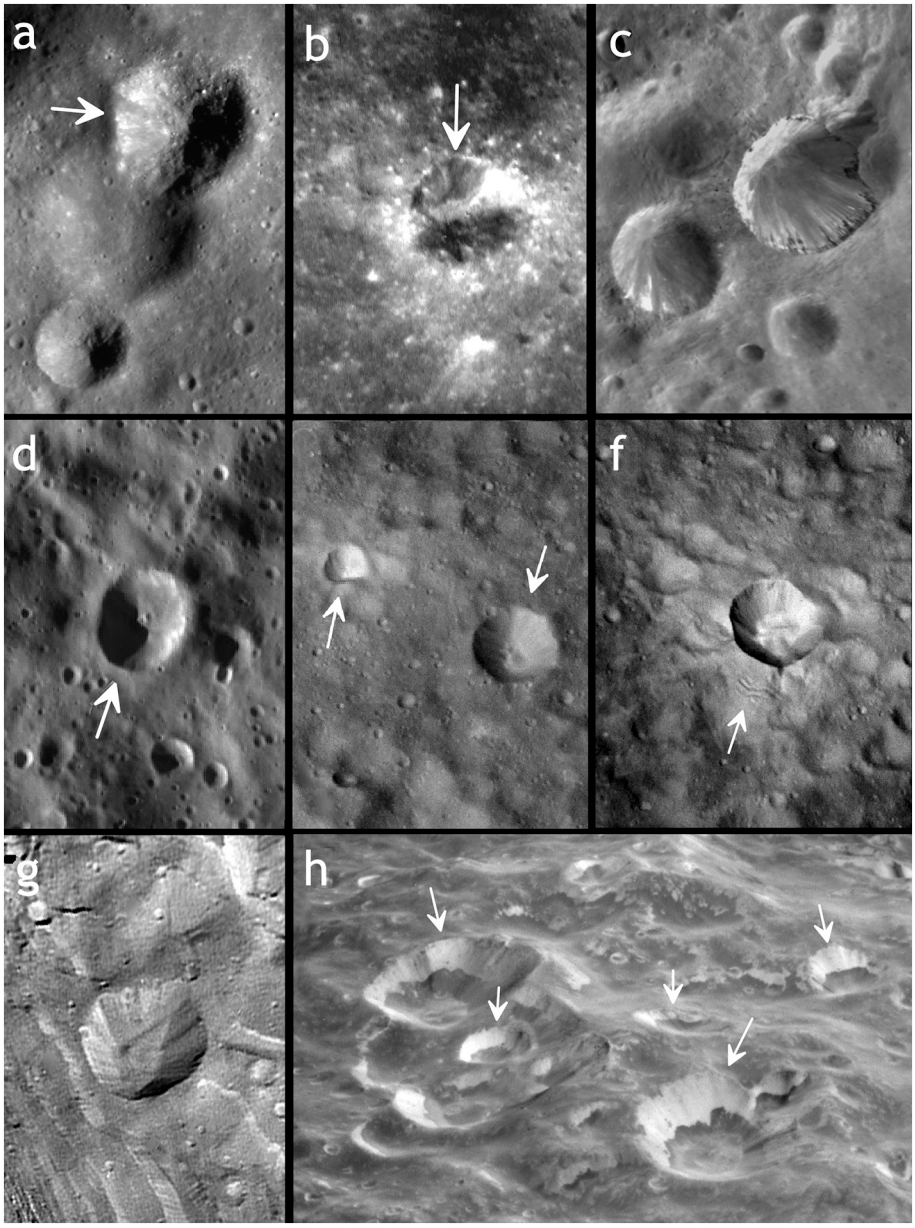

Fig. 8. Well-preserved simple craters on icy satellites. (a) 3.4-km-wide simple crater on Phoebe (arrow) with rubble-strewn rim at ~24 m GSD; (b) high-Sun image of 1.4 km simple crater on Phoebe with scarp (arrow) and rubble-strewn rim segments at ~13 m GSD; (c) 19 km Euphemus and 12 km unnamed sharp-rimmed craters on Phoebe with exposed coherent materials on rim scarp, at ~83 m GSD; (d) 2.5 km crater on Rhea (3N, 298E) at ~55 m GSD; (e) 2 km and 6 km simple craters on Dione (33N, 230E) at ~65 m GSD; (f) 10 km bright ray simple crater on Dione (32N, 225E) with exposed coherent materials on rim scarp and dune-like features in ejecta (arrow) at ~60 m GSD; (g) 24 km scarp-rimmed crater on Miranda at ~350 m GSD; and (h) oblique view of simple craters on Mimas from ~7 to 22 km in diameter at ~100 m GSD. These feature bright rim scarps (arrows) evident in high-Sun images of many craters in the Saturn system. Note that images are not shown to same scale but at approximate native image resolutions.

pit crater morphology seen on Ganymede (Schenk et al., 2018b). Thus the transition to central pits occurs at crater diameters of >350 km on the mid-sized icy satellites, or not at all.

3.5. Impact melt on icy bodies

Flat-lying depression filling deposits are essentially absent at impact craters on mid-sized icy satellites on either the floor or ejecta (Schenk et al., 2020a), with the dominant floor landform being the ridged floor units described above (Figs. 9, 10). Flat floor deposits in lunar craters (e.g., Fig. 3) are related to the deposition and solidification of impact melt or impact melt+debris in the lowest part of the crater due to its mobility during impact. This lack of flat-lying deposits either on crater floors or their ejecta on the Saturnian satellites or Charon indicates that either melt drains into fractures within the crater floor due to the higher density of liquid water (Senft and Stewart, 2011) or significant volumes of impact melt do not form on these bodies (Schenk et al., 2020a). We expect that basement fractures under the crater floor would tend to either close up quickly due to lateral compression, rapid freezing or would clog with debris to the point where at least some residual melt should remain on the surface. Even in a water ice target such a process is unlikely to be so efficient that cubic kilometers of a debris-rich impact melt would simply disappear underground leaving no significant material ponded on the surface. Lack of formation of impact melt on these satellites therefore seems more likely given that the floor and ejecta deposits of Inktomi, the prime example of an extremely fresh impact crater imaged at high resolution, lack any evidence of ponded material (Schenk et al., 2020a).

3.6. Transition diameters

Simple craters on the mid-sized icy Saturnian satellites (and Charon) have d/D ratios of ~0.2, similar within the uncertainties to the Moon (White et al., 2013, 2017). Complex crater d/D ratios are indeed shallower than simple craters but the slopes of the d/D curves are steeper (~0.5 to 0.6) than those for complex craters on larger icy satellites Ganymede and Callisto (White et al., 2013, 2017). The transition to immature complex craters on Dione and Tethys is ~10 ± 2.5 km for both

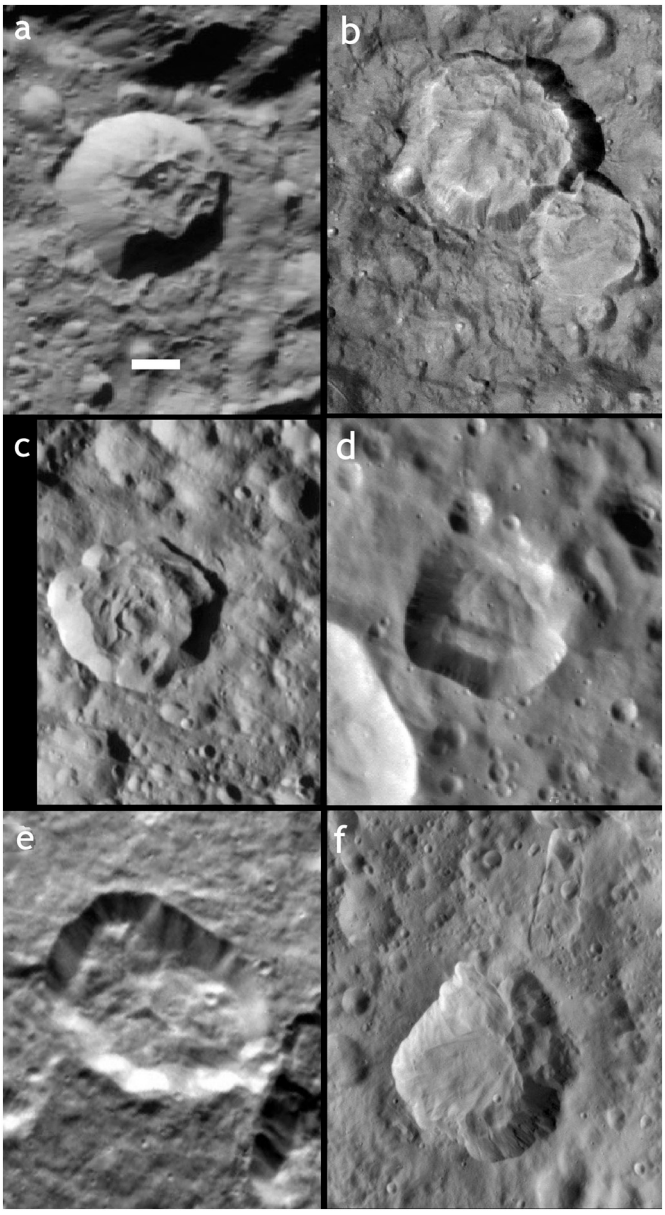

Fig. 9. Immature complex craters on various icy satellites. Craters sizes are: (a) 24 km (Tethys); (b) 28 km (Tethys); (c) 24 km (Tethys); (d) 24 km (Mimas); (e) 35 km (Dione); (f) 24 km (Tethys) crater formed on a ridge flank (note landslide originating from rim of smaller crater on top edge of frame). Images are approximately to scale; scale bar is 10 km.

bodies. The transition from immature complex craters to those with recognizable central peaks occurs at ~20 ± 5 km on Tethys and ~ 25 ± 5 km on Dione. Transition diameters and depth/Diameter statistics for these mid-sized icy bodies are discussed further in context with the Ceres data described below.

4. Crater morphologies on Ceres

Comparison of crater morphologies on Ceres to those of icy satellites are of interest because of Ceres' mixed crustal composition dominated by ice+clathrate with significant amounts of non-ice materials (Fu et al., 2017; Ermakov et al., 2017). Initial mapping results showed that craters on Ceres feature a progression of morphologies from simple to increasing complexity broadly similar to those on other bodies (Fig. 12; Hiesinger et al., 2016). Here we examine these findings in greater detail in light of the completion of global mapping at 35 m pixel scales, supplemented by limited coverage at 3.5 to 8 m pixel scales acquired during the extended mission phase.

4.1. Simple craters on Ceres

Simple craters are abundant on Ceres but at smaller diameters than on Vesta (Fig. 13); roughly <10 km diameter on Ceres compared to <35 km on Vesta (see also Discussion below on Transition diameters). Zeilnhofer and Barlow (2020) report d/D ratios averaging ~0.1. Our survey of pristine simple crater d/D ratios is approximately 0.2, near the lunar values, presumably because our sampling does not include more degraded craters. Unfortunately, current resolutions of pristine simple craters on the icy satellites (Fig. 8) are too low to allow detailed comparisons.

Although superficially similar there are significant differences in simple crater morphologies on Vesta and Ceres. Slope streaks and debris deposits are evident on rim wall slopes in fresh simple craters on Ceres, but these appear to lack the fine scale gullies and narrow finger-like debris flows common to Vestan simple craters (Figs. 1, 13) and resemble fan-like avalanches. As impact velocities are similar on these two bodies this might be attributable to composition-related mechanical or regolith fragment size differences. Although we do not make a detailed survey, Ceres craters also appear to feature more boulders per unit area and the upper 10% or so of rim wall slopes have greater proportions of knobby outcropping of coherent or resistant materials than on Vesta, again suggesting significant differences in regolith characteristics on the two bodies. Low-relief floor fill materials indicative of ponding of fluid or mobile debris at the bottoms of these craters is insignificant (Fig. 13), indicating that even less melt and/or debris accumulate in Ceres craters than on Vesta (Fig. 3). No evidence for pitted floor materials has been identified in simple craters on Ceres despite its high volatile content. More detailed study of these differences should be profitable.

4.2. Immature complex craters on CERES

Cerean immature complex craters in the diameter range from ~6 to ~20 km resemble immature complex craters on the icy satellites (Fig. 14) in most aspects: steep rim scarps, a lack of terracing, and hummocky floor materials comprised of irregular patterns of ridges, scarps and mounds. As on icy satellites, these craters also lack low-relief floor fill deposits at diameters <30 km (see next section). The floor hummocks and ridges in these smaller complex craters generally lack coherent or organized patterns, although a few display arcuate patterns (Fig. 14).

4.3. Mature complex craters on Ceres

As on icy satellites, larger mature complex craters on Ceres between ~20 and ~ 75 km diameters (Fig. 15) are basically similar to immature complex craters (Fig. 14), except for the presence of a recognizable central peak. In profile they usually have a rounded kinked "W" shape (Fig. 14) due to conical floor uplift and a lack of accumulated fluidized impact melt on the floor. The common break in slope of the bottom of the "W" is due to the accumulated ridge and scarp floor deposits near the base of the main rim scarp. In contrast to the immature craters, however, the floor hummocks and ridges tend to have more coherent or organized patterns involving concentric or spiral patterns (Figs. 14, 15). In some cases, these concentric ridges and scarps merge into and may be contiguous with partially developed terrace blocks in some craters. These more organized patterns may be related to uplift of the central peak, which tends to form or encourage radial merging into spiral patterns as observed in terrestrial complex craters (Kenkmann and Dalwigk, 2000; Kenkmann, 2002) and in laboratory experiments of converging materials (Allemand and Thomas, 1999). The lack of significant impact melt in many of these craters (see next section) allows the floor

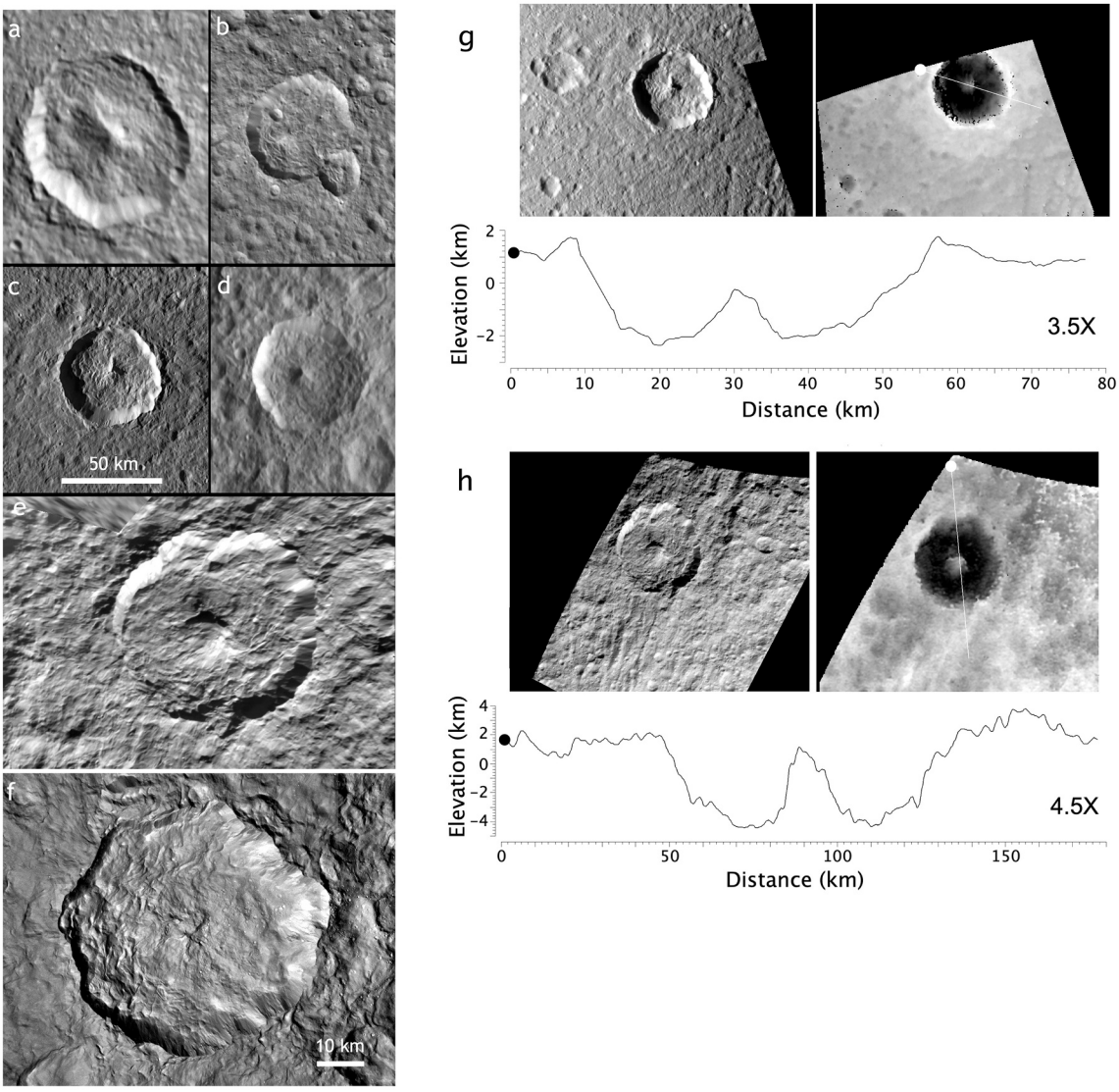

Fig. 10. (a–f). Mature complex (with central peak and floor deposits) craters on icy moons of Saturn. Named craters include (c) Sagaris, ~45 km (Dione) (e) Telemachus, ~95 km (Tethys), and (f) Inktomi, ~49 km (Rhea). Note arcuate scarps and ridges extending out from central peak of Telemachus (e) and other craters. All images shown to scale, except Inktomi. (g, h). Profiles of complex craters Sagaris (g) and Telemachus (h) on icy satellites Dione and Tethys, respectively. Inset map above profiles are from global image mosaic and DEM (Schenk et al., 2018b).

deformation patterns to be observed unobscured rather than be buried as in most lunar craters. These spiral patterns are addressed in more detail in Schenk et al. (Age and Formation of Rheasilvia Impact on Vesta and Launch of the HEDs, submitted Schenk et al., 2020b).

Some mature craters on Ceres exhibit narrow widely spaced concentric fractures <100 m wide several km long in a zone beyond the crater rim (Buczkowski et al., 2018; Otto et al., 2019). These features are apparently extensional and have been attributed to limited relaxation of the crater due to a shallow low viscosity subsurface layer at 1–2 km depths. The reduced viscosity is likely related to the presence of subsurface ices on Ceres. Similar features have not been detected on Vesta, nor the icy satellites (including at Inktomi; Schenk et al., 2020b). This would indicate a lack of a low viscosity subsurface layer on these bodies due to the non-ice composition of Vesta and the much colder or volatile poor subsurfaces of the icy satellites.

4.4. Larger mature complex craters on Ceres – impact melt

In contrast to icy satellites, larger mature complex craters on Ceres often exhibit relatively smooth floor-fill deposits that resemble impact melt deposits on other planetary bodies (Fig. 16). These floor fill deposits form as discreetly defined units that occupy the lowest parts of the crater, embay terrace blocks and other high standing structures, and are interpreted as impact melt. The 92-km Occator crater, target of Dawn's extended mission, is a classic example (e.g., Scully et al., 2019b; Schenk et al., 2019). As described by Schenk et al. (2019, 2020b) impact energies in larger craters on Ceres are sufficient to melt water ice and clathrates (e.g., Bowling et al., 2019) but no other components. Salts, phyllosilicates and perhaps carbonates will go into solution and unmelted clasts go into suspension, forming a slush- or mud-like mixture, which for convenience we will refer to as an impact melt-mixture. These mixtures are thus analogous to impact melt-debris mixtures found in large craters on other bodies such as Tycho, Ries, Manicouagan, and elsewhere in which the dominant crustal components are melted and other materials dissolved or suspended in solution. Of course, such deposits on Ceres will have their own distinctive composition, petrology, and rheology.

These impact generated floor deposits on Ceres are also often found stranded at higher topographic levels on terraces, including within Occator, consistent with emplacement of impact melts on the Moon and

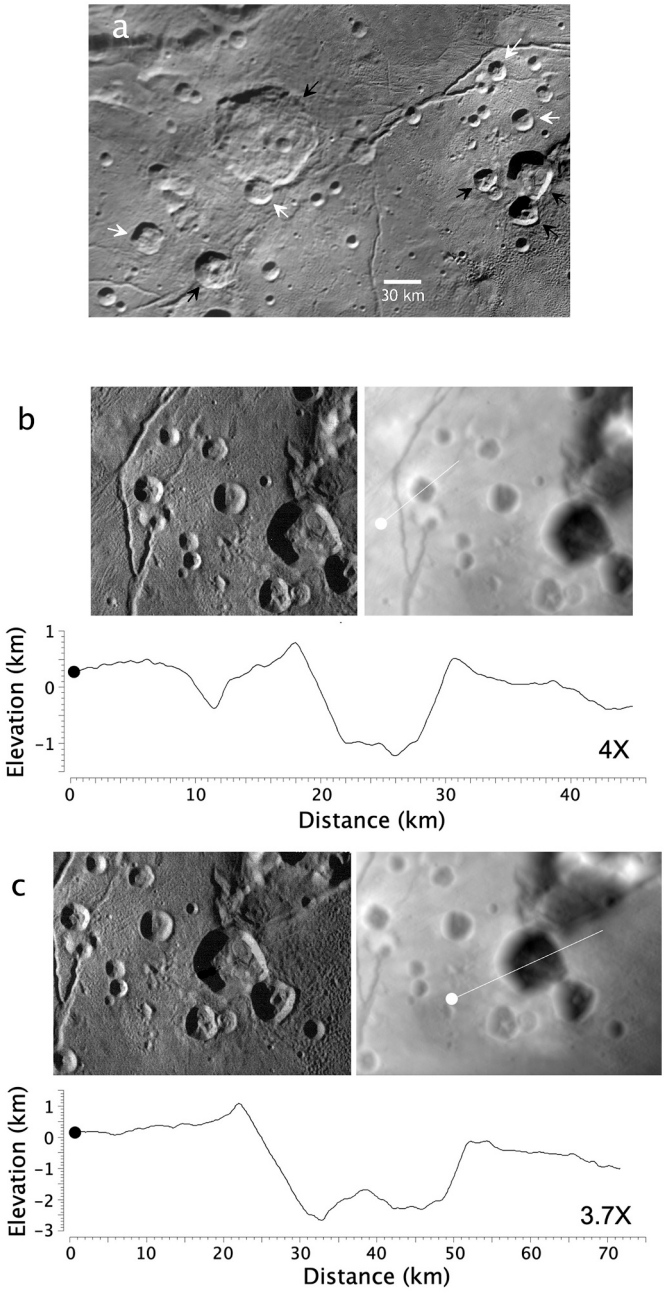

Fig. 11. a. Immature (white arrows) and mature (black arrows) complex craters on Charon. Right half of mosaic acquired at ~155 m GSD, left half at ~300 m. Mosaic centered at 3°S, 352°E and is 200 by 300 km across. b, c. Profiles of immature and mature complex craters on Charon. Topographic data and top insets are excerpted from global image mosaic and DEM of Charon (Schenk et al., 2018a). See a for location; north is to the left.

elsewhere (e.g., Schenk et al., 2019). Floor fill deposits occur in craters as small as 25 km (e.g., Kupalo, Haulani), but between 25 and 75 km such craters all occur at latitudes less than 45 degrees and for craters >75 km less than 65 degrees. This lack of impact floor deposits at higher latitudes indicates a possible internal thermal gradient control on melting due to colder polar surface temperatures. Zeilnhofer and Barlow, 2020) also cite evidence for latitudinal variations in the occurrences of some crater types as indicative of thermal differences on Ceres.

Some of these floor-fill deposits feature dispersed pitting (Fig. 17) that could be similar to volatile generated pitting observed in floor deposits of pristine Mars and Vestan (Fig. 2) craters (Sizemore et al., 2017). Some of these pits could be secondary craters that are common on Ceres, however. Terraces occur in roughly half of Ceres craters larger than ~35 km, and while broadly similar to those on lunar craters, the terrace blocks appear to be more disrupted or less coherent than on the Moon. Other than noting the general absence of terracing in icy satellite craters of any size (Figs. 9–10) and the possible influence of the strength of Ceres' non-ice components in lower strain rim failure mechanics, we do not discuss terracing in more detail here.

The 50-km-wide Ikapati crater is of interest for the large areas covered by smooth materials forming low-relief deposits perched at different elevations (Figs. 16–18). Like 75-km King crater on the Moon, Ikapati formed on the flanks of a larger older degraded basin, with impact melt-mixture accumulated asymmetrically on the lower slopes (Fig. 18). In a few areas, these deposits flowed through narrow channels to accumulate at lower areas (Fig. 17).

4.5. *Mature complex craters on Ceres: central pit (and peak ring) craters*

The occurrence of central pit craters on Ceres was a surprise due to their near total absence on the similar sized icy Saturnian satellites, based on the assumption that Ceres would behave more comparably to those bodies than to either the much larger Ganymede or Callisto (Schenk et al., 2019). As on Ganymede, Callisto (and Mars) pit morphologies on Ceres occur in two main types (Fig. 19), with a range of intermediate styles. Summit pits with high rims form on the tops of what are likely remnant central peaks. Floor pits are rimless depressions formed on the floors of craters, though these are sometimes flanked by irregular massifs forming an incomplete ring.

Simple g^{-1} extrapolation of the peak-to-pit transition diameters on Europa, Ganymede and Callisto of 22 to 35 km (Schenk, 1993) predicts central pit craters on Ceres at ~100–125 km diameters. Although many of the larger craters on Ceres are degraded or subsequent cratering obliterates their central structure, central pit morphologies are dominant in craters >75 km up to ~150 km, broadly consistent with inverse gravity scaling (see Discussion). As the Ceres images are the highest resolution images we have for central pit craters on any planetary body (except Mars, where formation processes may be different and erosion has modified the structures), these examples are important for understanding pit origins (e.g., Schenk et al., 2019).

Central pit crater Occator has been mapped in great detail (c.f., Scully et al., 2019, Scully et al., 2020b) and at very high resolutions (~3.5 m/pixel) due to the large carbonate deposits at its center. Because of its recent formation (~2 to 63 myr; Neesemann et al., 2019; Nathues et al., 2020) it is also the only crater larger than ~75 km that is very well preserved and whose original impact morphologies can be well mapped (Scully et al., 2019; Schenk et al., 2019; Schenk et al., 2020b). These include lobate floor deposits that flooded the southeast crater floor and are perched on the set of terraces over much of the rim scarp.

Central pits on Ceres display the full range of morphologies (Schenk et al., 2019) from nearly rimless floor pits (Gaue) to 3-km-high summit pits (Toharu). Like other central pits on Ceres, Ganymede and Callisto (Fig. 19), the Occator central pit is intermediate between these two extremes, with two asymmetric 1–3 km high massifs on either side of the shallow depression forming an incomplete ring. The central pit at Occator in thus not anomalous in a planetary context and Schenk et al. (2019) interpreted central pits on these three bodies as broadly equivalent within the context of lower imaging quality on Ganymede and Callisto, favoring uplift of a partial melted central structure from several kilometers below the surface. Occator is unusual in a Ceres context, however, for the preservation of a rounded fractured dome ~3 km wide and 750-m high in the central pit but such domes while non-existent on mid-sized icy satellites are common on Ganymede and Callisto at crater diameters >60 km (see Schenk et al., 2019 for discussion).

An additional transition may occur on Ceres. The largest recognizable central pit crater in our catalog is ~140 km across. The next larger craters that have not been heavily modified by infilling or cratering and

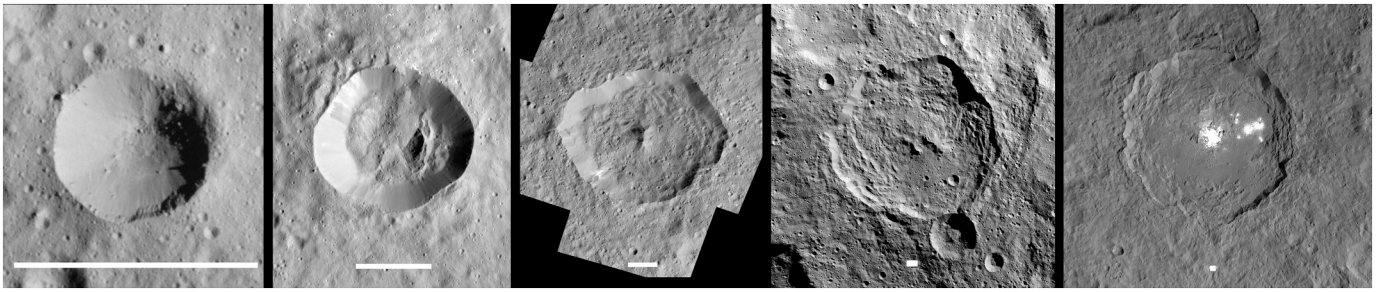

Fig. 12. Morphologic types of craters on Ceres, from ~3 to 92 km diameters, shown to similar apparent widths to compare internal structures. Fourth crater from left is Toharu (85 km) and fifth crater is Occator (92 km). Scale bar is 5 km.

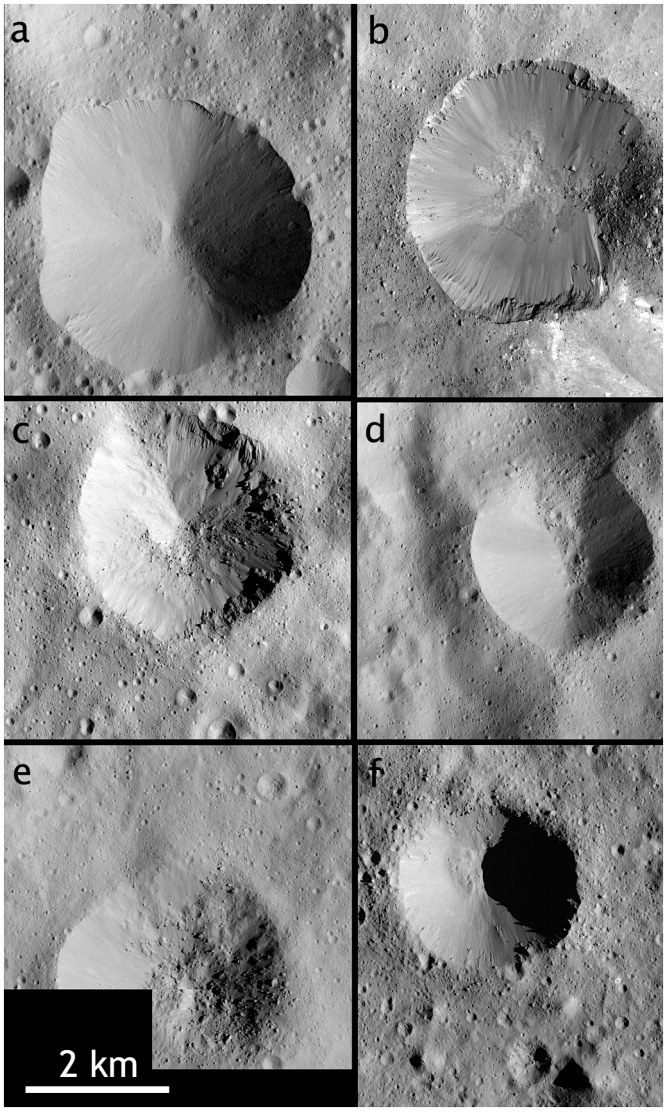

Fig. 13. Simple craters on Ceres in the 1–3 km size range. Note limited rim slumping and absence of floor fill deposits indicating lack of impact melt. Images acquired at ~3.5 to 8 m/pixel and shown approximately to scale. Scale bar is 2 km.

can be classified are ~165 km diameter Urvara and 270 km Yalode (Buczkowski et al., 2016; Crown et al., 2018). Urvara features a complex internal morphology of linear ridges and knobby peaks and does not conform to either central peak, central pit or other classifications. There is a central smooth area ~ 20 km across flanked by irregular low knobs and massifs, suggestive of a very poorly developed or preserved central pit, however. Yalode features a nearly complete inner ring ~100 km across in the form of a low rise ~1 km high and scattered modified knobs. This wide ring is more similar in relative scale to the peak rings of large lunar craters (e.g., Schrödinger) rather than the smaller central pits, although it appears to be significantly modified by 'smooth material' (Crown et al., 2018). As Yalode is approximately twice as large as the next largest classified basin, it probes deeper into Ceres and may be influenced by the rheological properties of the weaker brine-rich zone or the stronger hydrated mantle (e.g., Castillo-Rogez et al., 2019). Impact modeling that tests central uplift or relaxation in a layered Ceres is required to evaluate the relevance of Yalode, although the occurrence of only one classifiable basin of this size limits any conclusions that can be drawn.

4.6. *Simple-complex transition diameters on Ceres*

Four transitions are documented on Ceres in well-preserved craters: the d/D curve inflection point, simple-to-complex, immature-to-mature (central peak) complex, and central peak to central pit (Fig. 20). These are measured at 6.3 ± 2 km, 7.5 ± 2.5 km, 20 ± 2.5 km, 75 ± 15 km, respectively (Fig. 21). The transition on Ceres from melt-poor to melt-rich morphologies occurs at ~30–75 km diameter (and larger than those for immature and central peak morphologies). Staggered transitions for structural elements (terraces, peaks, melt-mixtures) are also observed on the Moon and Mercury (Pike, 1980) as each collapse element is influenced by different factors. The similarity of the Ceres simple-to-complex transition at ~7.5 km to those on icy satellites was reported by Hiesinger et al. (2016), but the similarities of the other transitions complete the survey. The depth/Diameter curve for complex craters (Fig. 20) is shallower on Ceres (best-fit slope of ~0.38) than for similarly sized icy satellites (White et al., 2013, 2017). This can be attributed at least in part to shallowing of larger craters by floor deposition of impact melt-mixtures in Ceres craters and/or greater development of rim terraces that both widen and flatten, neither of which are observed on icy satellites. These and other morphologic differences are discussed in the next section.

5. Comparative crater morphologies on low-gravity bodies

The rich data sets recently acquired for Vesta, Ceres, and the mid-sized icy Saturnian and Plutonian satellites provide a natural laboratory for comparison of impact crater morphologies formed under a variety of conditions and crustal compositions. As these bodies share similar gravity, it allows us to investigate and better understand the impact processes and target properties driving differences and similarities in the crater properties (Table 1) independent of surface gravitational acceleration. The differences in crater morphology with increasing diameter are especially of interest as they probe more deeply into and potentially reveal differences between the interiors of these bodies.

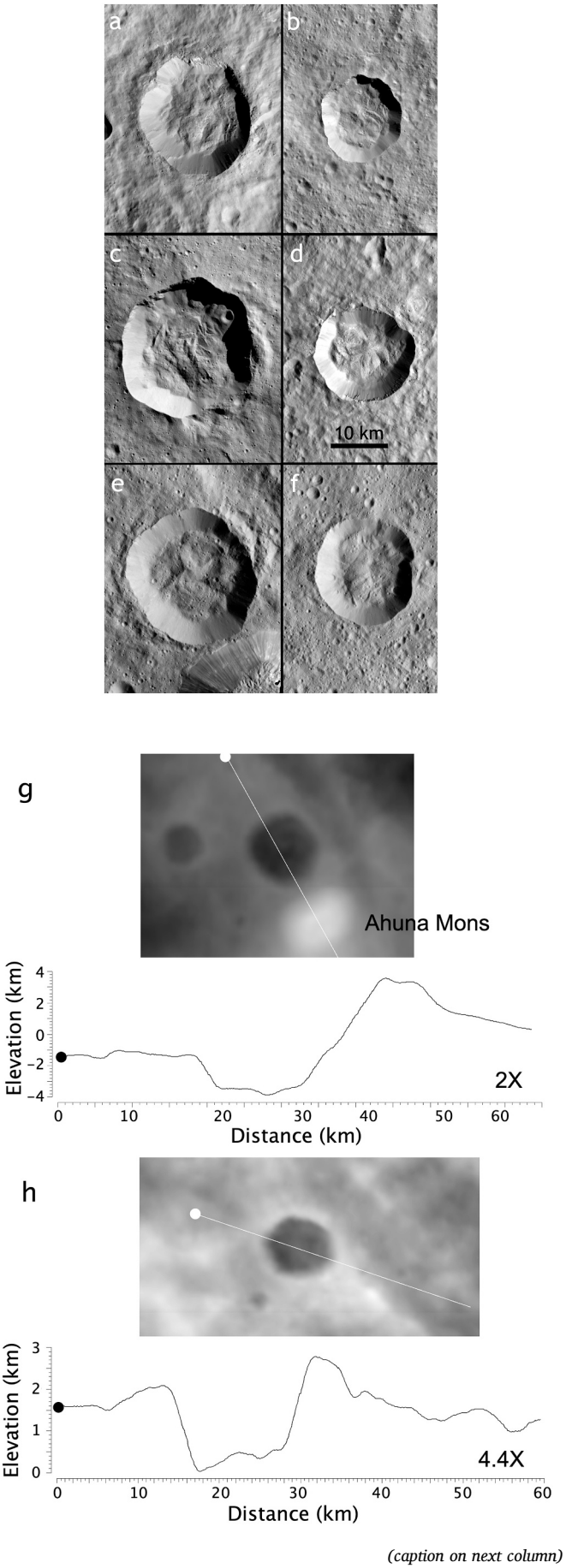

(caption on next column)

Fig. 14. (a–f). Immature complex craters on Ceres. All images acquired at 35 m GSD and shown to scale. (a) 15 km (23S, 279E); (b) 10 km (26S, 191E), note arcuate ridges extending from center; (c) 17 km (40S, 110E); (d) Cacaguat, 13.5 km; (e) 18 km (8S, 315E), note Ahuna Mons at lower right; (f) 14 km (6N, 89E). (g,h). Profiles of two immature craters on Ceres. Crater in Fig. g lies adjacent to the base of Ahuna Mons, the high mound at lower right in that scene. Inset images above profiles are from global DEM (Roatsch et al., 2016).

5.1. Asymmetric craters

A peculiarity of Vestan craters is the apparent abundance of "asymmetric" craters. These are craters with distinctly different rim morphologies in different (usually opposing) radial sectors of the crater (Fig. 22) and that are usually found on significant slopes (Krohn et al., 2014b). The two primary morphologies are sharp striated rim scarps which form an abrupt cliff (common to larger simple craters) and often feature narrow low volume debris slides along the scarp face, and on the other side a rubble-strewn rounded rim with no abrupt scarp. The percentage of rim circumference represented by these two types of morphologies can range from ~5% rubble-strewn to >70% rubble-strewn (Fig. 22), with the rubble-strewn morphologies always on the side of the crater that is lower in elevation. In some craters, striated rim wall scarps are apparent along lower parts of a rim segment, which transition into a rubble-strewn morphology near the rim crest (Fig. 22). Craters smaller than ~0.75 km are usually mostly of the rubble-strewn rim type. On Vesta these asymmetric craters occur in the 0.3 to ~43 km diameter range (Krohn et al., 2014b) with the large spread due mostly to the highly variable relief of Vesta's surface. Most craters were formed on slope angles >10° with a steady decrement to lower slope angles (Krohn et al., 2014b).

Krohn et al. (2014b) has looked at asymmetric craters on Vesta and concluded that the rubbly sides of the crater were due to fallback of ejecta onto the rim, due to a combination of the fast rotation period and the steep slopes on which most of these craters formed on Vesta. While this effect is likely real it does not account for the presence of a sharp rim scarp and related slumping on the uphill rim sections and rounded rubbly rim scarps on the downslope section (Fig. 22). Nor does it account for the observation that all-rubble-strewn rim morphologies are more common at smaller crater diameters and scarp morphologies at larger diameters generally. A search of the lunar imaging catalog from Lunar Reconnaissance Orbiter reveals similar asymmetric craters on the Moon, as well as smaller craters that are entirely dominated by the rubble-strewn rim morphology (Fig. 23). Our very limited survey suggests that asymmetric craters are common on the Moon at roughly 0.5 to 1-km diameters but can occur in larger craters (e.g., Hawke, D ~ 13 km) depending on local elevation differentials.

Asymmetric craters on Ceres (Fig. 24) are on similar slopes as on Vesta but typically only 0.3–4.2 km across (Krohn et al., 2019) and thus approximately 10 times smaller on average than on Vesta. The Ceres examples are only resolved well in the extended mission phase when resolutions improved to 3.5–8 m/pixel but are generally similar in morphology. The majority of asymmetric craters on Ceres appear at slope angles between 5 and 20 degrees. Few such craters are identified on icy satellites, where identification is hampered by resolution limits and the low numbers of well-resolved pristine craters. We observe several asymmetric craters on Phoebe (Fig. 8), with an apparent transition from rubbly to scarp-cut rims at ~4 ± 2 km.

We propose that the rubble-strewn rim morphologies represent preserved portions of the transient cavity in the absence of rim failure and slumping. The rubble is thus fragmented target material that did not have sufficient velocity to escape the crater floor during the excavation phase (with perhaps some additional fallback ejecta). Rim failure along scarp faces normally occurs within larger simple craters to produce debris slides (e.g., Figs. 1, 2), but not in those rim segments where rounded rubble-strewn rim morphologies are preserved. This rim failure debris is more voluminous in lunar and terrestrial simple craters (such as

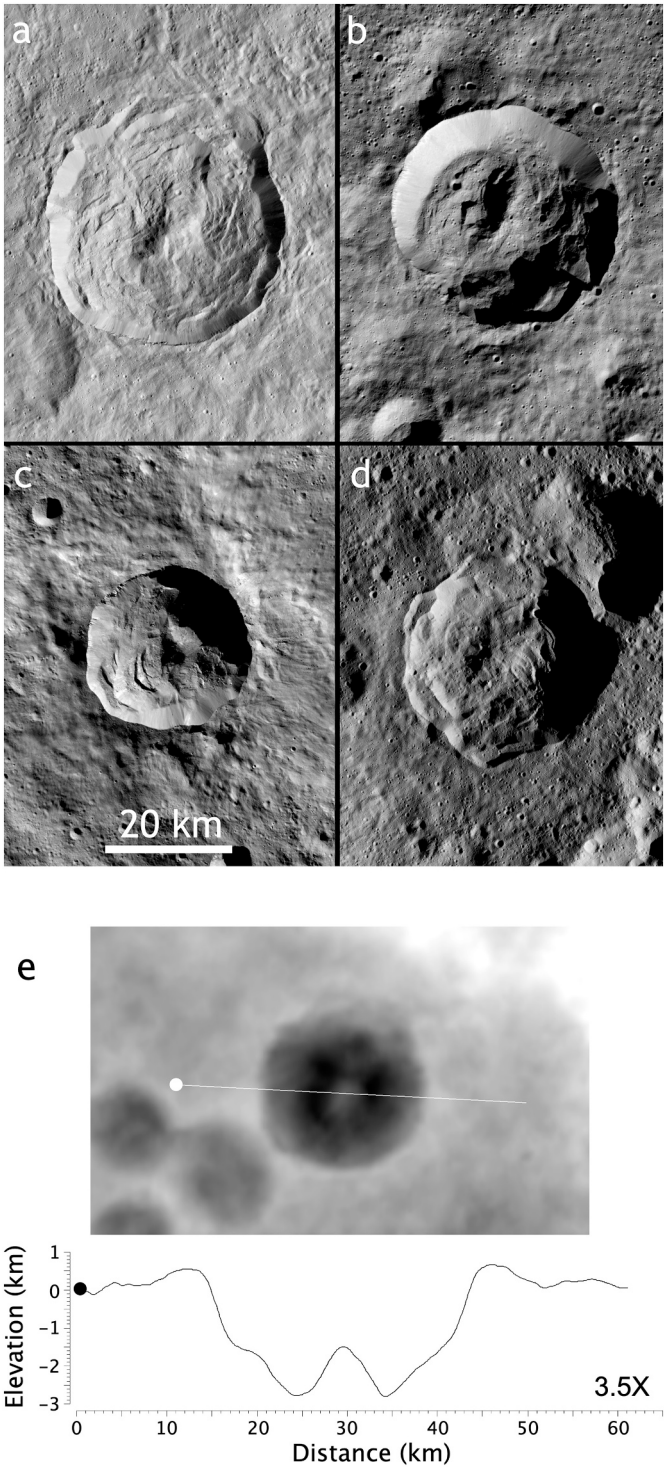

Fig. 15. (a–d). Mature complex crater on Ceres. Craters: (a) Kokopelli, 46 km, 18N, 125E; (b) Laukumate, 29 km, 64N, 160E; (c) Nunghui, 21 km, 54S, 271E; (d) unnamed, 27 km, 68N, 350E. Images to scale. (e) Profile of crater Kokopelli, Ceres. Inset map above profile is from global DEM (Roatsch et al., 2016).

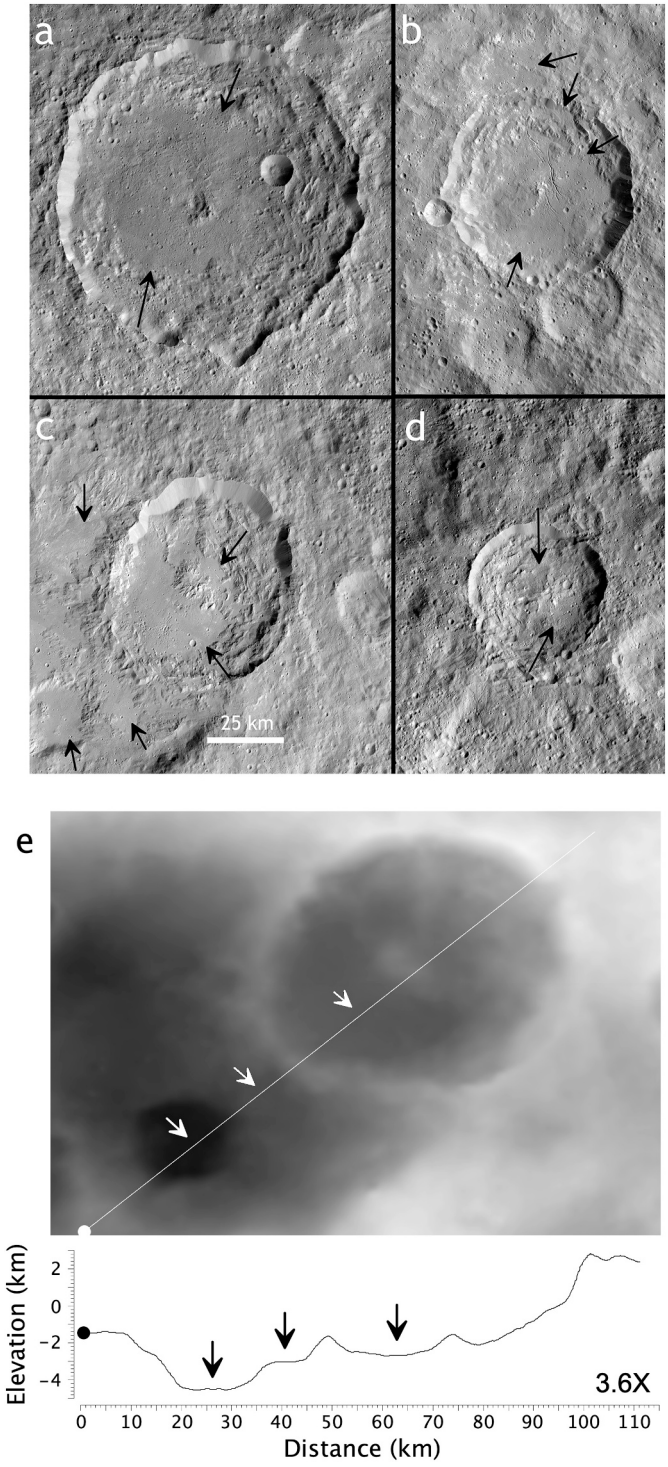

Fig. 16. (a–d). Large mature complex craters on Ceres with varying extents of smooth floor deposits interpreted as impact melt-mixture (arrows). (a) Gaue, ~79 km, note central pit with partial rim massif to southeast; (b) Azacca, ~54 km; (c) Ikapati, ~50 km; (d) Aristaeus, ~37 km. Images to scale. Compare with Fig. 10 showing a lack of similar deposits on icy satellites. (e) Profile of Ikapati and southwest ejecta/melt deposits. Arrows indicate deposits perched at different elevations. Top inset is from global Ceres DEM (Roatsch et al., 2016).

Meteor Crater and G. Bruno) than on Vesta or Ceres, contributing together with impact melt to form the extended breccia lens at the bottoms of such craters (Fig. 3; cf. Melosh, 1989).

Formation on regional slopes can result in asymmetric craters with lower rim slopes and lower effective rim-to-floor height differentials on the down-slope side than on the up-slope side. Overburden stresses within the rim of the transient cavity are proportional to ρgh (Melosh, 1989), where ρ is density, g is density, and h is crater depth. This is undoubtedly an oversimplification due to the presence of a slope in vacuum and other factors but is useful as an approximation to the effective strength of impact disrupted materials. Smaller and shallower craters do not exceed this threshold and retain their original transient

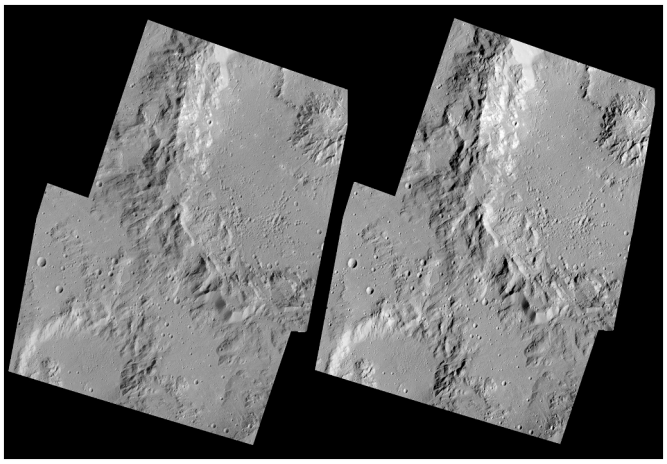

Fig. 17. Stereo view of southwest quadrant of 50-km-wide Ikapati crater and its ejecta, showing smooth material ponded at multiple topographic levels, including smaller areas perched on the rim crest. Several channel-like cascades are evident at bottom center where materials flowed over rim into the small degraded crater at bottom left. Images at ~35 m GSD.

shapes and rubble-strewn rims. Larger craters exceed the failure criterion everywhere on the rim and have well developed failure scarps. Those craters close to the required ρgh threshold for failure would be more likely to display mixed morphologies (Fig. 24) depending on local conditions and the effective rim height around the circumference. In cases of craters on significant slopes we infer that the formation of rim failure and scarp formation on the uphill portions of crater rims is due to higher stress levels at the rim base given their greater height (Fig. 25). The portion of the rim on the lower side has a lower effective height and does not exceed the failure stress and so retains an intact rubble-strewn morphology. With the lower surface gravity on Vesta, craters near the threshold of rim failure are larger and frequently occur on steeper regional slopes than commonly observed on the Moon. Vesta is unusual in its high proportion of steeper slopes relative to crater diameter (Krohn et al., 2014b) resulting in craters with asymmetric rims.

Transition from rubble-strewn to scarp rim morphologies is very broad due to variable slopes on planetary surfaces. While a detailed survey of these craters is not within our scope, we also find that the transition from rubble-strewn to scarp rim morphologies in lunar and Cerean simple craters tend to be considerably smaller than the Vesta examples, consistent with higher gravity on the Moon and weaker rheology on Ceres (where gravity is similar the Vesta). Using our provisional transition diameters represented by asymmetric simple craters on the Moon, Vesta, Ceres and Phoebe (~1 km, ~15 km, ~1.5 km, and ~ 4 km respectively but uncertain to within roughly 50% due to our small samples), and reasonable values for crustal density with low porosity, we find that the critical failure strengths (ρgh) on each body are on the order of $\sim 10^6$ Pa for the Moon and Vesta but $\sim 10^5$ Pa for Phoebe and Ceres, respectively. Pending more complete global surveys, our transition diameter estimates are at least consistent with upper icy layers on planetary bodies (including Ceres) having effective material strengths during impact an order of magnitude lower than silicate rich bodies.

5.2. *Crustal composition of Ceres and Vesta*

The crater modification process of floor uplift and rim failure involves deformation in a large quasi-hemispheric zone beneath the impact site and is hence controlled by and reflects the material properties within that zone. Like the Moon and Mercury, Vesta's crust has negligible water ice content (e.g., Sarafian et al., 2019). Gravity, density and shape analyses indicate that water ice, and perhaps clathrates, together constitute ~70–80 vol% of Ceres crust, the remainder being salts, carbonates and phyllosilicates (Fu et al., 2017; Ermakov et al., 2017). The large differences in morphologies and transitions diameters on Vesta and Ceres discussed throughout this report (Figs. 1, 4, 14–16) indicate that a much weaker material (namely water ice) is rheologically dominant on Ceres during impact compared to volatile-depleted Vesta, as surface temperatures, mean impact velocities and projectile densities are all very similar on the two bodies. The d/D transition diameter of 29 km and simple-to-complex morphology transition of ~35 ± 5 km for Vesta are factors of 2 to 3 smaller than expected from a g^{-1} extrapolation of transitions on the Moon and Mercury (Fig. 7). The fit to the transition diameters for silicate-rich bodies including Vesta suggests a dependence

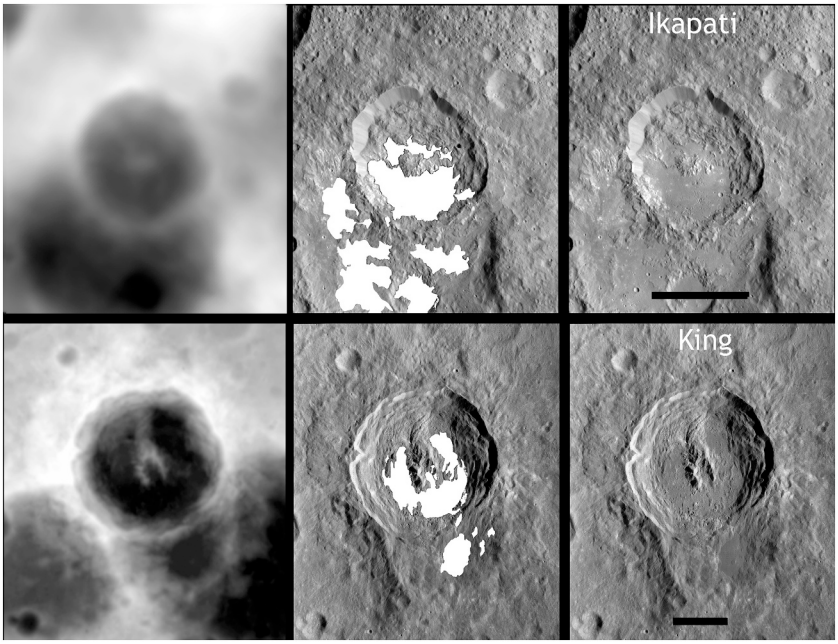

Fig. 18. Comparison of smooth material distribution on 50-km Ceres crater Ikapati (top) and 75-km lunar crater King (bottom). Panels are: (left) topography (dark is low; range shown is 4 km); (center) images with low-relief melt units in white; (right) original images. Scale bars are 40 km for both craters.

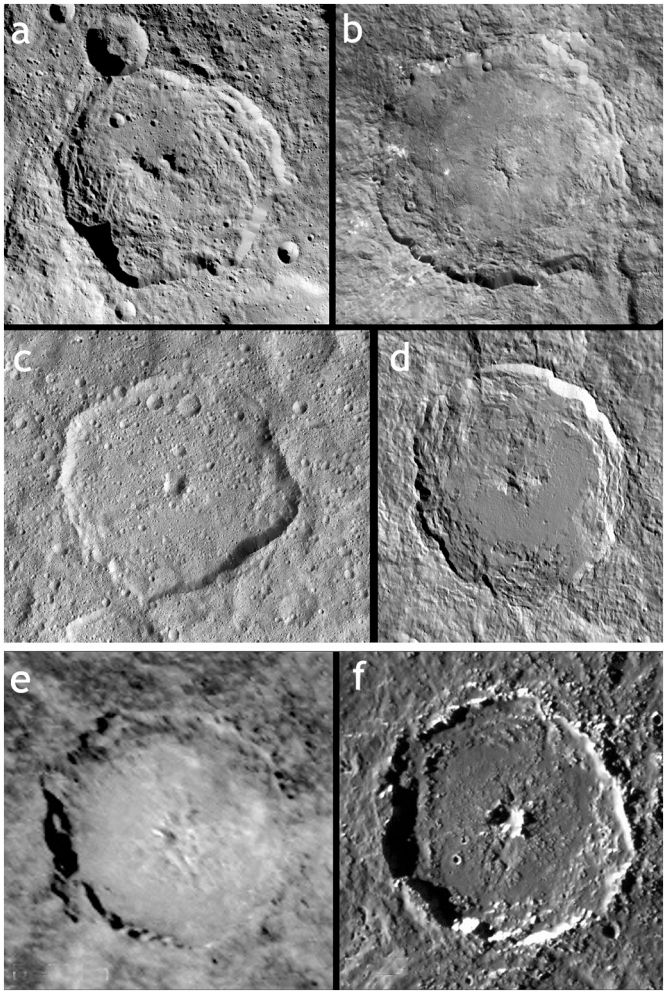

Fig. 19. Central pit craters on Ceres (top two rows) as compared to Ganymede and Callisto (bottom row). Ceres (top rows): (a) Toharu, 82 km, with summit pit; (b) Dantu, 119 km, with floor pit; (c) Nawish, 77 km; (d) Occator, 92 km (shown as shaded relief of topography due to high contrast of central pit). Ganymede and Callisto (bottom row): (e) central pit crater on Ganymede, 70 km, with floor pit; (f) central pit crater on Callisto, 65 km, with floor pit and partial rim massif to the east, similar to Occator. See also central pit crater Gaue (Ceres) in Fig. 16. Images are not to same scale.

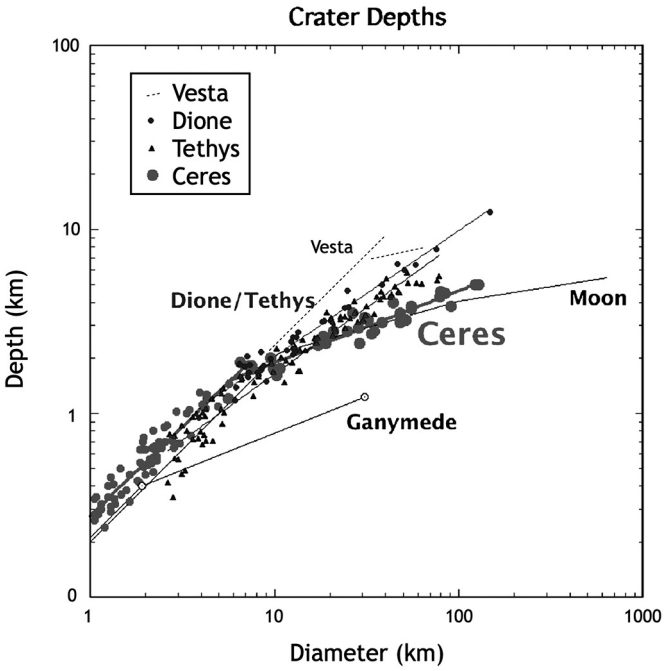

Fig. 20. Depth to diameter measurements for fresh craters on Ceres. Thin dashed lines are best fits to Vesta data from Fig. 7. Dione and Tethys data from White et al. (2017), Ganymede best fit from Schenk (2002).

of $g^{-0.65}$ but relies on a single data point. Whether Vesta's smaller transitions are due to unknown effects of low gravity on crater modification processes in silicate rich targets, or to peculiarities of Vesta's composition or differences in porosity that weaken the crust is not known.

Impact melt deposits do occur on Vesta (Williams et al., 2014a) in the form of small surficial flows or minor accumulated floor deposits (Figs. 1, 3). The low volumes of accumulated impact melts on Vesta relative to the Moon (e.g., Figs. 1–3), however, are consistent with predictions that lower impact velocities will result in lower melt production than on Vesta (Keil et al., 1997). Porosity should tend to increase melt production relative to the Moon (cf. Williams et al., 2014a) but the low melt volumes observed on Vesta, even at scaled crater diameters, suggests that porosity may not be very different on the two bodies.

Our comparisons of craters on Ceres and the icy satellites reveal basic similarities in morphologies and transitions (Figs. 26, 27). All four major transition diameters obtained for Ceres are statistically indistinguishable from the icy satellites of Saturn and Pluto (Fig. 27). Consistent with this is the indistinguishability of central peak dimensions on Ceres (i.e., width and height) from those on icy satellites (Fig. 28). While peak widths on these bodies are broadly similar (perhaps a few & larger) to those on the Moon, peak heights are roughly 20–50% larger than on the Moon (e.g., Baker and Head, 2013), in part due to the greater volumes of impact melt flooding crater floors on the Moon. The similarities of landforms and transitions are fully consistent with an ice-rich composition for the outer layers of Ceres as determined from shape and gravity (Fu et al., 2017; Ermakov et al., 2017) down to depths of several 10's of kilometers if not deeper (given the involvement of large volumes beneath the crater). Although present in greater quantities on Ceres, it is evident that non-ice materials such as salts and phyllosilicates do not control the fundamental initiation of complex crater morphologies represented by the transition diameters in Fig. 27, but that the much weaker rheologic strength of water ice does. We explore implications of crater morphology for Ceres' interior more in the next two sections.

5.3. *Impact melt(−mixture) deposits on Ceres*

Despite the similarities in transition diameters indicating a dominant role for water ice in crater formation on Ceres and the ice satellites, we also observe important morphologic differences likely related to composition, internal thermal or rheologic structure, or possibly impact velocity. At diameters above ~25 km, aspects of crater morphology on Ceres diverge from those on icy mid-sized satellites. The common occurrence of impact melt-mixture floor deposits at crater diameters greater than ~25 km and especially >75 km (Figs. 10, 16) is in stark contrast to the lack of preserved melt deposits on mid-sized icy satellites (Schenk et al., 2020b). Deposition of larger amounts of melt materials at the bottom of larger craters would tend to decrease the apparent crater depths on Ceres relative to Tethys or Dione, possibly explaining the shallower d/D slope for complex craters on Ceres (Fig. 20). Unfortunately, current resolutions are insufficient to unambiguously verify the formation of melt deposits on Ganymede and Callisto.

The occurrence of melt-rich complex craters at diameters >30 km indicates that impacts in the crust of Ceres reached a threshold which permits melting that does not appear to occur on most icy satellites. Impact energies are sufficient to melt water ice (Bowling et al., 2019; Hesse and Castillo-Rogez, 2019) and clathrate hydrates on Ceres. Though not melted by impact heat, salts and other minerals will be put

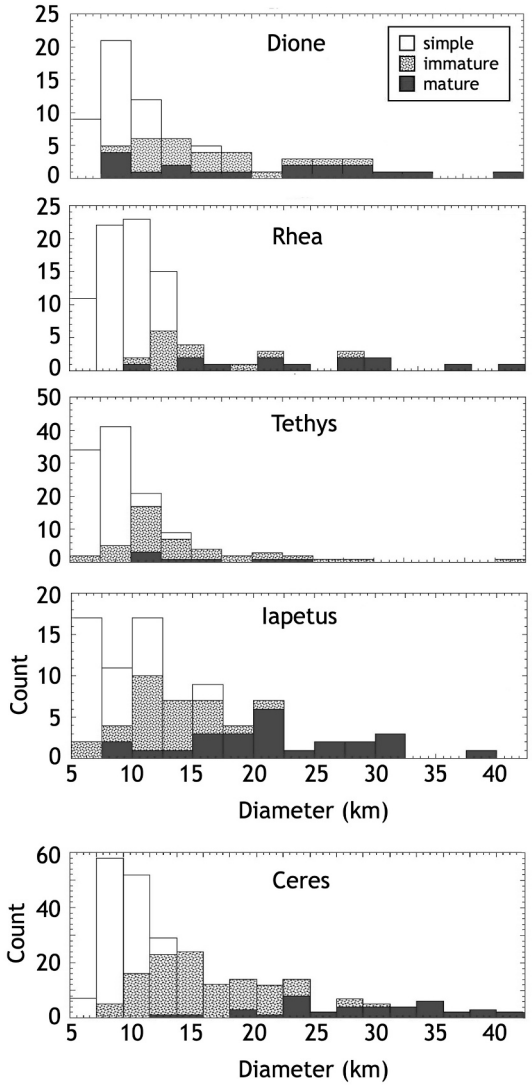

Fig. 21. Histograms of morphology crater types on icy satellites and Ceres. Types include simple bowl (white) and immature floor hummocks (hatched) and mature central peak (dark) complex.

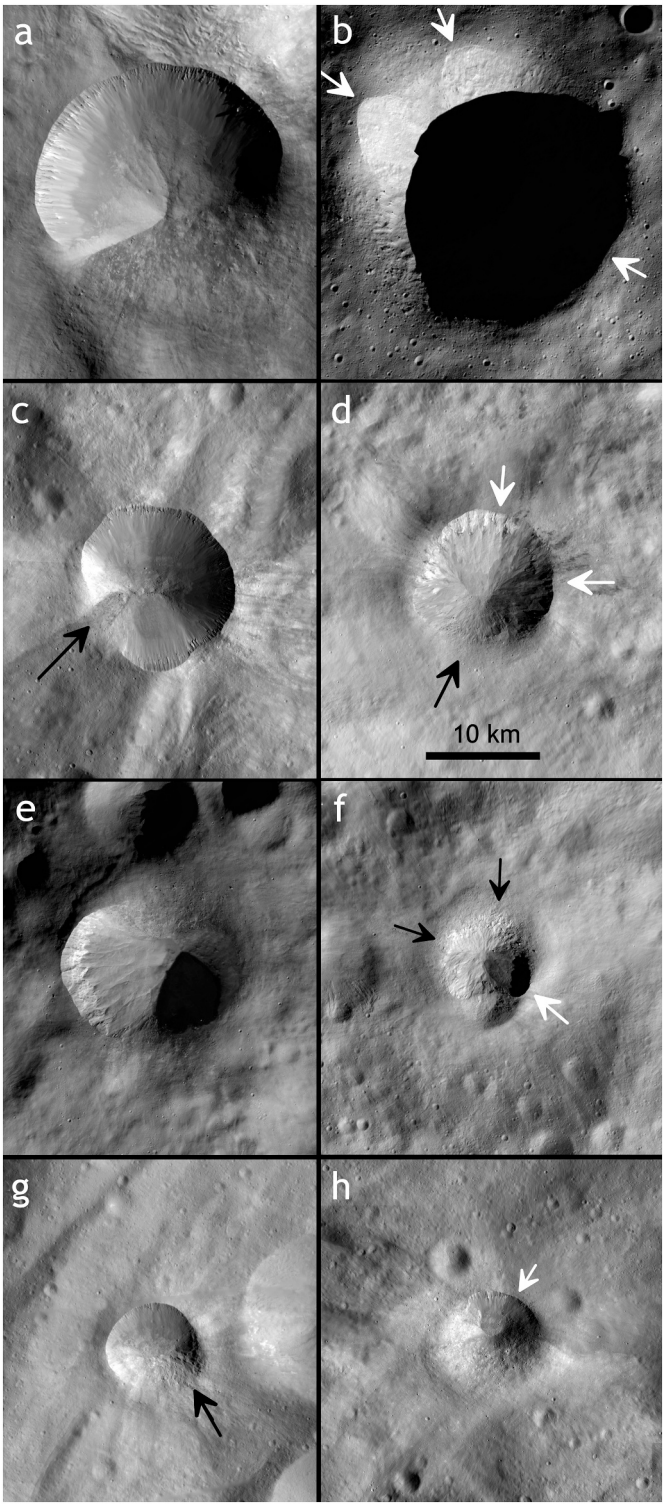

Fig. 22. Asymmetric simple craters from on Vesta. Craters: (a) Antonia, ~17 km; (b) Scantia, ~20 km, (c) Canuleia, ~11 km; (d) Rubria, ~10 km; (e) Fabia, 12 km; (f) Teia, ~7 km; (g) Charito, ~7 km; (h) Justina, 7 km. Black arrows highlight rubbly rim segments, white arrows to rim segments with partial scarp formation. Images shown to same scale.

into solution or suspension in such melts, producing a Ceres-specific melt-mixture. Melt-mixtures on the icy satellites are more likely to involve water mixed with lower temperature phases such as methane or ammonia in various minor amounts depending on satellite composition.

The lack of impact melt or melt-mixtures on the icy satellites and frequent occurrence on Ceres is of interest as it appears to be contrary to expectation, given that higher velocity encourages melt production generally (e.g., Pierazzo et al., 1997). Mean heliocentric impact velocities on Ceres are ~5 km/s (but with a spread of velocity of roughly ±3 km/s [Williams et al., 2014a), while on the icy satellites they range from ~2 km/s at Charon to 6–30 km/s at Saturn (Singer et al., 2019; Zahnle et al., 2003). Impact velocities can vary by factors of ±3 on opposite sides of synchronously rotating bodies such as the Moon or the icy satellites, and by other effects such as projectile approach geometries. Thus melting of ice would be expected in volumes perhaps as large as in lunar craters if comets produced most Saturn system craters (Schenk et al., 2020b). We note that impact melt deposits are mappable at Mannanan crater on Europa (cf. Schenk and Turtle, 2009), indicating that they are and should be preserved on icy bodies. A significant fraction of Saturnian craters might be formed by lower-velocity planetocentric impactors (e.g., Kirchoff et al., 2018; Bell, 2020; Ferguson et al., 2020). Secondary and sesquinary craters derived from large impact basins such as Odysseus are possible (Schenk et al. 2018) but are very unlikely to be larger than 20 km across and not relevant to the lack of larger melt craters. Zahnle et al. (2003) and Alverellos et al. (2005) estimate impact velocities of Saturn orbiting projectiles in the range of 1 to 4 km/s, comparable to those on Charon (Singer et al., 2019) and overlapping

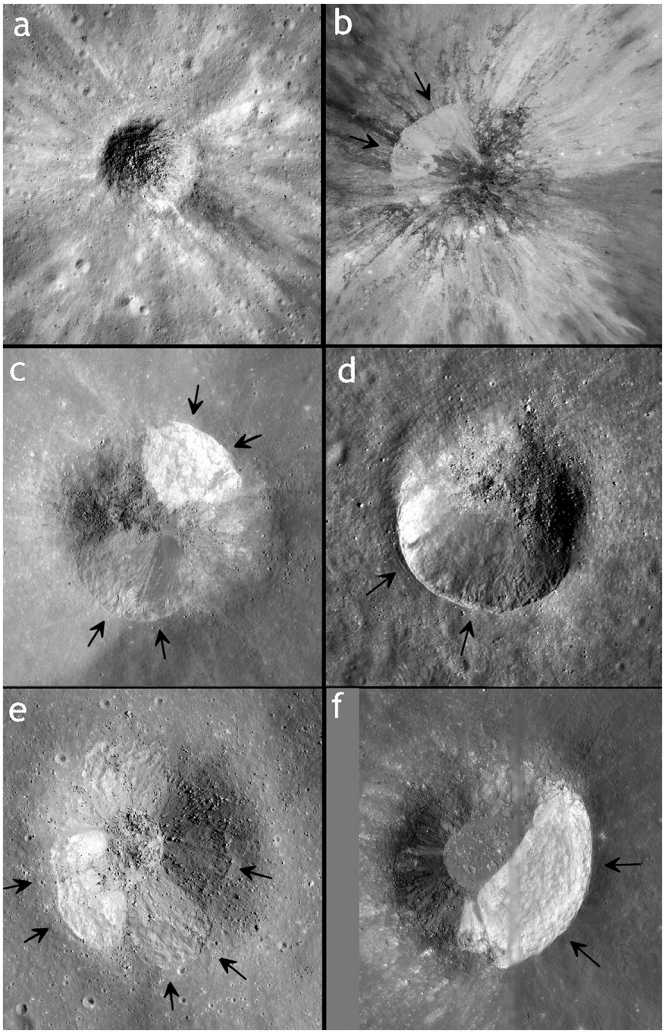

Fig. 23. Asymmetric craters on the Moon. The 190-m crater (a) has rounded rubble-strewn rim. The 800-m crater at 3S, 37E (b) occurs on a gentle rise with the scarp-cut rim on the uphill (left) side. High solar illumination highlights albedo contrasts. The 2-km crater (c) at 2.1N, 79.4E formed atop a narrow low ridge crossing from lower left to upper right, with the highest portions of the rim coinciding with the two opposing areas of rim scarp formation (arrows). Crater (d) is 700 m across and formed on the sloping southwest wall of Harvey crater. The 950-m North Ray crater (e) has partially developed rim slump scarps in an irregular pattern (arrows indicate areas of rim scarp development). Nearby South Ray crater at 700 m is mostly a rubble-strewn rim type. The 4-km crater (f) at 9.3S 74.7E occurs on the side of a low rise with the scarp rim on the high (right) side. Another classic example is the 8 km asymmetric crater on the east rim of Lowell crater. Images are not all to same scale due to resolution differences.

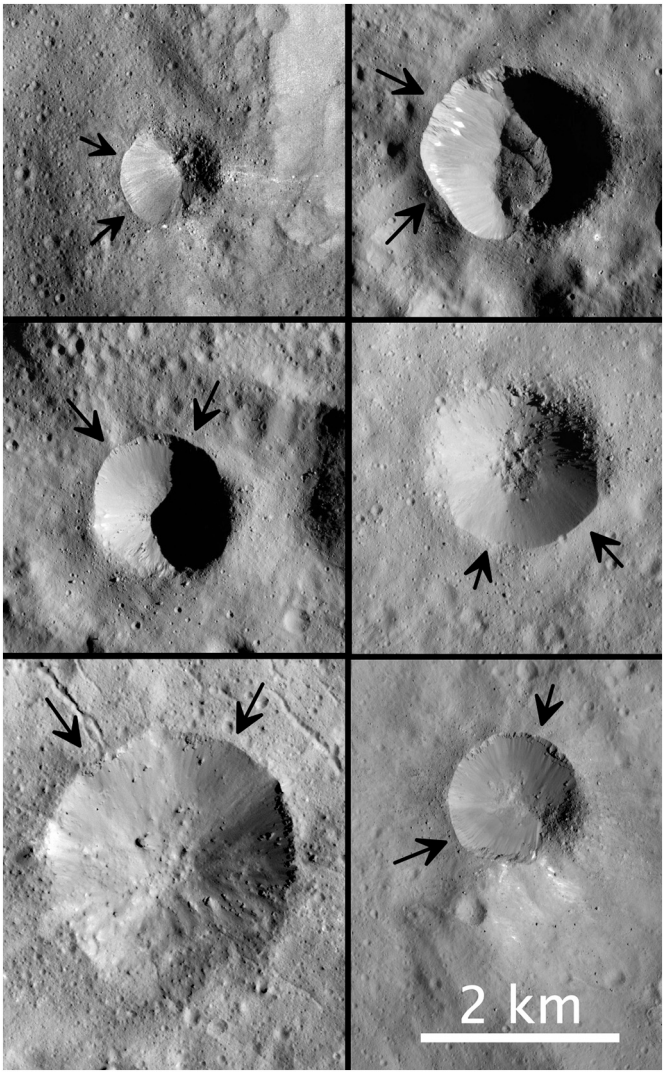

Fig. 24. Asymmetric craters on Ceres. Craters approximately to same scale; scale bar is 2 km. Arrows indicate rim segments with well-developed scarps.

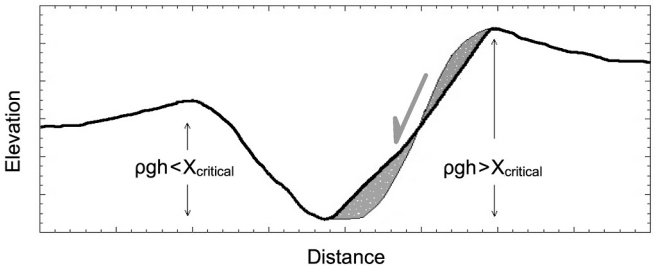

Fig. 25. Schematic illustration of principle of asymmetric overburden rim failure in simple craters on slopes. $X_{critical}$ is proportional to the failure criterion for impact disrupted crustal material. At smaller diameters $X_{critical}$ is not exceeded (or is at larger diameters) anywhere in the crater.

with the lower range of velocities at Ceres.

The relative contribution of planetocentric debris to the cratering records at Saturn remains unresolved but is unlikely to be the dominant source of craters >20 km (Kirchoff et al., 2018), the size range of interest here for melt production. At present there is no compelling evidence that such debris is the only source of craters or that comets are not responsible for the younger well-preserved craters in the Saturn system (Kirchoff et al., 2018), suggesting that there should be at least some larger craters formed by heliocentric impactors in Saturn system with impact melt deposits as extensive as those on Ceres (ignoring for the moment internal temperature differences). Given its extremely young age, the 49-km Inktomi crater and its extensive bright ray system is likely of higher velocity cometary origin but as with others, this crater appears to be free of accumulated impact melt (Schenk et al., 2020b).

Higher density asteroidal objects likely dominate the flux at Ceres (e.g., O'Brien et al., 2014) in contrast to the comets that dominate on icy satellites (Kirchoff et al., 2018), but projectile density is likely only a minor contributor to relative melt production (Pierazzo et al., 1997; Cintala and Grieve, 1998; Plescia and Cintala, 2012) compared to projectile mass and velocity. Hence, we consider that low velocity impactors may not explain the well documented lack of ponded impact melts

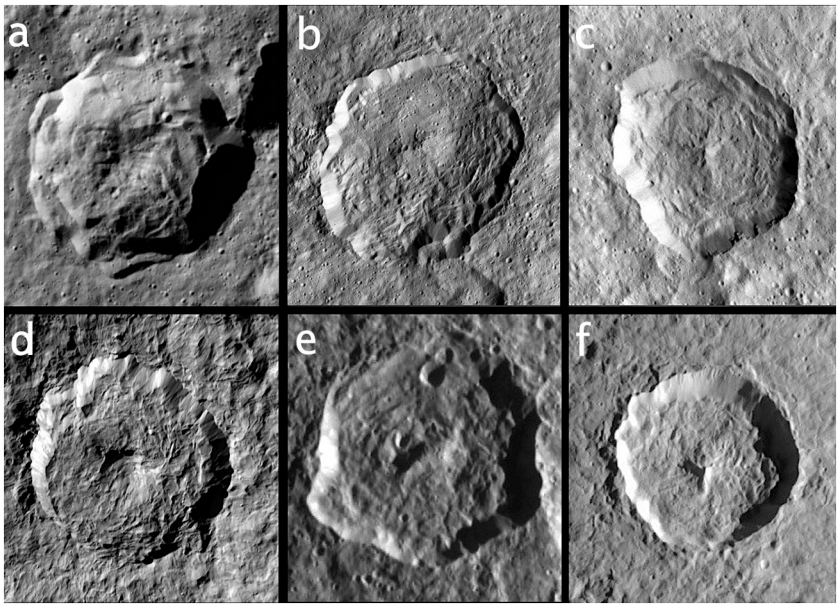

Fig. 26. Comparison of immature complex craters on Ceres (a–c) and on icy Saturnian satellites (d–f). Ceres craters are between 20 and 40 km across. Crater (d) is Telemachus (D = 95 km) and (f) is Sagaris (D = 45 km), also highlighted in Fig. 10. Craters shown at similar apparent diameter (and at different scales) to facilitate structural comparison.

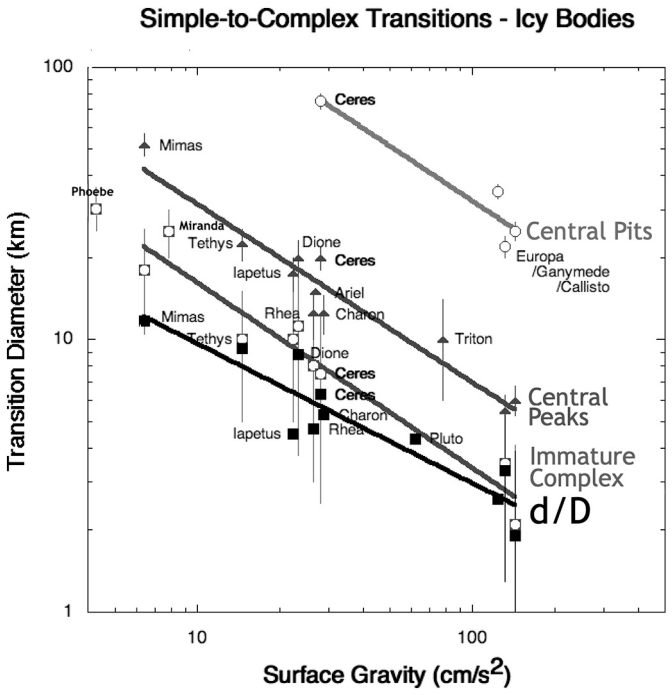

Fig. 27. Transition diameters for crater types and depth/diameter inflection on Ceres and icy satellites. Lines are best fits through data.

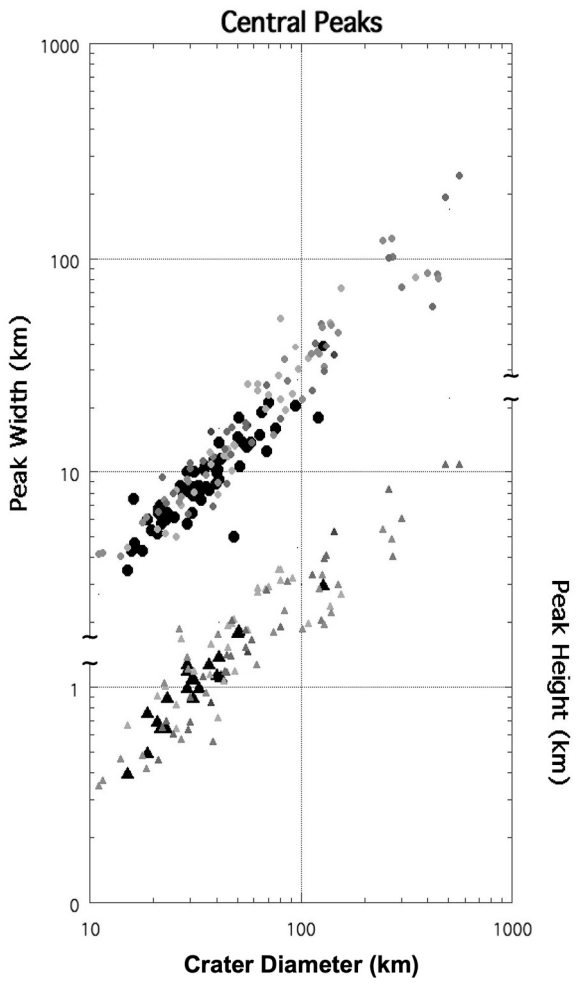

Fig. 28. Central peak dimensions on icy satellites and Ceres. Upper trend is form peak widths, lower for peak heights. Small grey points are for icy satellites Mimas, Tethys, Dione, Rhea and Iapetus; larger black points for Ceres craters.

at Inktomi and all other large fresh craters in the Saturn system (Schenk et al., 2020b).

The other major differences are mean surface temperatures (~165 K on Ceres, <100 K at Saturn and beyond). Near-surface temperatures on Ceres below the skin-depth (~155 K) may not be that much different from Saturnian satellites, but a shallower thermal gradient (higher internal temperatures) is expected in Ceres if liquid water remains below the crust (e.g., Castillo-Rogez et al., 2019). This and the lack of impact melt deposits in craters at very high latitudes (poleward of ~70°) on Ceres (Schenk et al., 2019) would suggest that internal temperature

gradients are the more likely controlling factor in melt production.

Regardless of the final answer, the observational lack of impact melt in craters in the Saturn system places important constraints on the impact process and target properties. Whether steeper temperature gradients, differences in impact velocity (which are confused by potential orbiting debris in the Saturn system), compositional complexity or a combination of factors enables large-scale impact melt or melt-mixture formation on Ceres will require numerical modeling or experimentation beyond our scope here.

5.4. Transition diameters and central pits on Ceres

Our transition diameters on Ceres are indistinguishable from icy satellites (Fig. 27), implying a high-volume fraction of water ice on the body and consistent with internal models (e.g., Ermakov et al., 2017). Impact experiments and models suggest that 30 vol% non-ice material in an icy crust could still result in craters that are indistinguishable from those formed in pure water ice, other factors being similar, likely because grain-to-grain interactions of stronger materials likely become rheologically important only in the >30 (or perhaps 50) vol% range under impact conditions (Gareth Collins, pers. comm).

Despite the high ice+clathrate composition of the crust from gravity and shape data, the preservation of crater relief against low strain viscous relaxation implies a crustal ice content on Ceres of only 40 vol% (Bland et al., 2016), in seeming contradiction to our conclusions based on pristine morphology. Although not well calibrated under impact conditions, it seems likely that the weakest material (i.e., ices, clathrates) will control the behavior of craters under the extreme strain rates associated with impact, at least until the stronger material reaches a critical volume percentage, while the stronger (non-ice) crustal components dominates rheologic response under the much lower strain rates associated with relaxation. Under high strain, clathrate cages are crushed and it converts to ice, releasing volatiles. These factors explain how Ceres' crust can contain significant amounts of non-ice material in the form of clathrates and produce primary crater morphologies that so closely resemble those on icy satellites, and yet stiffen the ice shell sufficiently to prevent pervasive low strain viscous relaxation of large craters over the age of the Solar System (Bland et al., 2016). The apparent discrepancy can be explained if the ~60 vol% non-ice component required by the viscous relaxation constraints includes significant quantities of clathrates to a total of ~80 vol% ice plus ice-clathrates.

Although the simple-to-complex transition diameters using our four criteria on the icy targets in our study are consistently along similar trends (Fig. 27) the gravity dependence on these transitions is not −1 but −0.65 (except for the d/D transitions which have a $g^{-0.5}$ dependence). The order of magnitude lower values of the icy versus silicate transition diameters (Schenk, 1991) remains valid as indicative of the fundamental weak rheology of water ice-rich crusts. The somewhat weaker than −1 dependence on gravity for transitions on icy bodies (Fig. 27) is similar to that suggested for silicate bodies by the single Vesta point (Fig. 7). This somewhat weaker dependence on *g* suggests that, while surface gravity dominates, additional factor(s) are influencing the various simple-to-complex transitions. One possible factor could be (as yet undocumented) increasing porosity with lower gravity, if it has the effect of weakening effective target strength during impact.

The fact that central pits similar to those observed on Ganymede and Callisto are observed on Ceres (and at similar gravity scaled diameters) but not at all on Saturnian satellites (Figs. 9, 10, 23) (Schenk et al., 2019) also reveals a fundamental difference between Ceres and these satellites. Central pits could be related to the melting of significant volumes in the localized region of the central uplift (cf. Schenk et al., 2019). Using the same crude scaling inferences as above that crater modification involves a zone comparable in depth to its diameter, the prevalence of central pits to ~140 km could also imply an ice-rich layer to a comparable depths on Ceres. This is deeper than the average thickness of the crust/ice layer of ~40–55 km as inferred from gravity and shape (Ermakov et al., 2017) and might instead support the model by Mao and McKinnon (2018) who suggested that a small non-hydrostatic anomaly in Ceres' shape is a fossil bulge from a period when Ceres was spinning faster by ~30 min.

Central pits could also be related to target layering as suggested by Greeley et al., 1982) and indicate a weak layer at depth. At Ceres, the existence of such a layer has been inferred from the combination of admittance and topography relaxation analysis to start at about 40 km depth on average (Ermakov et al., 2017; Fu et al., 2017). The density of this layer inferred by Ermakov et al. (2017) is about 2400 kg/m^3. Its viscosity is poorly constrained at $<10^{20}$ Pa s (Fu et al., 2017). Hence the fraction of liquid mixed with the rock is poorly constrained from geodynamical modeling alone. Additional information may come from modeling the rock density using available mineralogical and geochemical constraints (see Castillo-Rogez et al., 2018). A brine-rich layer may extend deeper than 100 km, below which topography relaxation modeling loses sensitivity (Fu et al., 2017). The approximate inverse gravity scaling of the central pit transition diameters of the large Galilean satellites and Ceres (Fig. 27) would then be a coincidence. Conversely, the "melted central peak" model for central pit formation could be effective on Ceres due to the higher internal temperatures in the uplifted central peak materials, at least in comparison to the colder icy satellites of Saturn (see discussion in Schenk et al., 2019). The interiors of Ganymede and Callisto are likely significantly warmer than those of the smaller Saturnian satellites, which in combination with higher impact velocities could favor melt and central pit formation there, and on Ceres assuming it is also warmer than Saturnian satellites (Senft and Stewart, 2011).

In summary, the first-order similarity of craters on Ceres and icy satellites at all diameters indicates that water ice plus ice-clathrate is the dominant rheologic phase in Ceres' crust but that additional factor(s) modulate crater formation. Temperature gradients and/or rheologic layering (such as a brine-rich layer below Ceres' crust) may be controlling factors in impact melt-mixture and central pit formation at diameters of >30 km and > 75 km respectively on these lower gravity bodies but will require numerical and physical modeling. There may be other dissimilarities including the greater development of concentric terrace blocks in Cerean craters (Fig. 14), which may be related to the mixed crustal composition of Ceres, that also need to be considered in evaluating Ceres crater morphologies.

6. Conclusions

Impact craters on Vesta, Ceres, and the icy satellites of Saturn, Uranus and Pluto form a natural laboratory in impact mechanics as these bodies all have similar surface gravities but different compositions ranging from ice-rich satellites to virtually ice-free Vesta. There are many aspects of crater morphology such as ejecta, boulders, fracturing, color and compositional variations, not addressed here but our comparative analysis of crater shapes and morphologies on these bodies will provide a framework for these more detailed analyses.

Simple craters on these bodies are broadly similar in most aspects, (given differing resolutions on all the target bodies) but there might be more boulders and less floor fill for Ceres simple craters than on ice-free Vesta. Asymmetric craters, in which part of the rim is a rounded rubble-strewn ridge, the rest a sharp-rimmed scarp (Figs. 23–25), occur on all these bodies and are likely due to differential overburden stress in tilted craters on slopes. The smaller diameter occurrences of these asymmetric craters on Ceres and Phoebe is broadly consistent with icy targets being an order of magnitude weaker than non-ice planetary targets. Concentric and spiral patterns in the ridge and scarp floor deposits of complex craters are common on Ceres and icy satellites and similar to that observed on Vesta's Rheasilvia basin. The occurrence of these patterns in nature and experimentally indicates they result from deformation mechanics of converging fractured solid materials during impact events and support a young age for Rheasilvia (Schenk et al., submitted,

2020b).

Ceres crater morphologies are to first order very similar to icy satellites at all diameters but very different from Vesta, despite identical surface gravity. These include the transitions from simple-to-complex, complex to central peak, and central peak to central pit, as well as depth/diameter inflection points (Figs. 7, 27). Although there is some variability among the target bodies, simple-complex transitions for ice-rich bodies including Ceres follow $\sim g^{-0.65}$ trends (except d/D which is closer to $g^{-0.5}$). This indicates that all these bodies including Ceres have outer shells rheologically dominated by a very weak material under impact conditions, compared to Vesta or the Moon. These findings are consistent with independent morphologic and compositional evidence for large amounts of water ice in the crust of Ceres. Corroborating evidence includes large lobate landslides (e.g. Schmidt et al., 2017; Chilton et al., 2019), fluidized ejecta (Hughson et al., 2019a), flexed topography (Hughson et al., 2019b), floor-fractured and concentrically fractured craters (Buczkowski et al., 2018; Otto et al., 2019; Krohn et al., 2020), pitted terrain (Sizemore et al., 2017), limited viscous relaxation (Bland et al., 2016), possibly hydrologically-derived domes and tholi (e.g. Schmidt et al., 2020; Sori et al., 2017), and the spectral detection of large amounts of near-surface hydrogen (Prettyman et al., 2017), all of which are absent on Vesta. The indication of strengthening from lack of viscous relaxation, however, requires a stronger non-ice material and limits water ice to ~40 vol% (Bland et al. (2016). This apparent conflict can be resolved if Ceres' crust is 80 vol% ice plus clathrate (e.g., Hesse and Castillo-Rogez, 2019), with the latter reverting to or behaving like water ice under impact conditions, resulting in impact craters similar to those on icy satellites. Ice dominates rheologic response under high impact strains but non-ice components dominate under the much lower strains during creep.

One major exception to the similarities in morphologies is the preservation of impact melt in Ceres craters >30 km in diameter (Figs. 10, 16), attributed to the effects of either higher surface and internal temperatures or larger proportions of non-ice components in Ceres' crust, or on the melting criterion during impact, or a combination of these effects. The lack of melt deposits in polar craters on Ceres and total lack on the mid-sized icy satellites (Schenk et al., 2019) suggests thermal gradients may be the stronger influence on melt production. Terrace blocks may be more common in larger craters on Ceres than they are on icy satellites and this might be attributable to compositional differences.

The other major difference is the occurrence of central pits on Ceres and Ganymede and Callisto at diameters approximately consistent with inverse gravity scaling (Fig. 27), but not the mid-sized icy satellites. This too might be attributable to the influence of higher internal temperatures, but also possible layering at comparable depths in Ceres, including a transition to a lower crust enriched in brines. Despite the fundamental similarities of Ceres and icy satellite craters demonstrating the controlling influence of the weak rheology of water ice on impact processes on those bodies, the observed differences also illustrate the influence of compositional and thermal differences among planetary bodies.

Declaration of Competing Interest

None.

Acknowledgements

The author thanks the NASA Dawn Participating Scientist Program and the Dawn project for financial support. LPI Contribution No. 2551. LPI is operated by USRA under a cooperative agreement with the Science Mission Directorate of the National Aeronautics and Space Administration.

References

Allemand, P., Thomas, P., 1999. Small scale models of multiring basins. J. Geophys. Res. 104, 16501–16514.
Alverellos, L., Zahnle, K., Dobrovolskis, A., Hammill, P., 2005. Fates of satellite ejecta in the Saturn system. Icarus 178, 104–123.
Baker, D., Head, J., 2013. New morphometric measurements of craters and basins on Mercury and the Moon from MESSENGER and LRO altimetry and image data: An observational framework for evaluating models of peak-ring basin formation. Planet. Space Sci. 86, 91–116.
Bell, S., 2020. Relative Crater Scaling Between the Major Moons of Saturn: Implications for Planetocentric Cratering and the Surface Age of Titan. J. Geophys. Res 125, e2020JE006392.
Bland, M., Raymond, C., Schenk, P., Fu, R., Thomas, Kneissl, Pasckert, J., Harry, Hiesinger, Preusker, F., Park, R., Marchi, S., King, S., Castillo-Rogez, J., Russell, C., 2016. Composition and structure of the shallow subsurface of Ceres revealed by crater morphology. Nat. Geosci. 9, 538–542. https://doi.org/10.1038/ngeo2743.
Bowling, T.J., Ciesla, F.J., Davison, T.M., Scully, J.E.C., Castillo-Rogez, J.C., Marchi, S., Johnson, B.C., 2019. Post-impact thermal structure and cooling timescales of Occator crater on asteroid 1 Ceres. Icarus 320, 110–118. https://doi.org/10.1016/j.icarus.2018.08.028.
Buczkowski, D.L., 24 others, 2016. The geomorphology of Ceres. Science 353. https://doi.org/10.1126/science.aaf4332.
Buczkowski, D.L., Sizemore, H.G., Bland, M.T., Scully, J.E.C., Quick, L.C., Hughson, K.H.G., et al., 2018. Floor-fractured craters on Ceres and implications for interior processes. J. Geophys. Res. 123, 3188–3204. https://doi.org/10.1029/2018JE005632.
Castillo-Rogez, J.C., Neveu, M., McSween, H.Y., Fu, R.R., Toplis, M.J., Prettyman, T., 2018. Insights into Ceres' evolution from surface composition. Meteorit. Planet. Sci. 53, 1820–1843.
Castillo-Rogez, J.C., Hesse, M., Formisano, M., Sizemore, H., Bland, M., Ermakov, A., Fu, R., 2019. Conditions for the long-term preservation of a deep brine reservoir in Ceres. Geophys. Res. Lett. 46, 1963–1972.
Chilton, H.T., Schmidt, B.E., Duarte, K., Ferrier, K.L., Hughson, K.H.G., Scully, J.E.C., et al., 2019. Landslides on Ceres: inferences into ice content and layering in the upper crust. J. Geophys. Res. 124, 1512–1524. https://doi.org/10.1029/2018JE005634.
Cintala, M., Grieve, R., 1998. Scaling impact melting and crater dimensions: implications for the lunar cratering record. Met. Planet. Sci. 33, 889–912.
Cintala, M., Wood, C., Head, J., 1977. The effects of target characteristics on fresh crater morphology: preliminary results for the Moon and Mercury. Proc 8th Lunar Sci Conf. Geochim. Cosmochim. Acta (Suppl. 8), 3409–3425.
Clayton, J., Osinski, G., Tornabene, L., Kalynn, J., Johnson, C., 2013. Fresh transitional lunar impact craters. In: 44th Lunar Planet. Sci. abstract. 2345.
Combe, J.-Ph., McCord, T.B., Tosi, F., Ammannito, E., Carrozzo, F.G., De Sanctis, M.C., Raponi, A., Byrne, S., Landis, M.E., Hughson, K.H.G., RAymond, C.A., Russell, C.T., 2016. Detection of local H2O exposed at the surface of Ceres. Science 353. https://doi.org/10.1126/science.aaf3010.
Combe, J.-P., Raponi, A., Tosi, F., De Sanctis, M.C., Carrozzo, F.G., Zambon, F., Ammannito, E., Hughson, K.H.G., Nathues, A., Hoffmann, M., Platz, T., Thangjam, G., Schorghofer, N., Schröder, S., Byrne, S., Landis, M.E., Ruesch, O., McCord, T.B., Johnson, K.E., Singh, S.M., Raymond, C.A., Russell, C.T., 2019. Exposed H2O-rich areas detected on Ceres with the dawn visible and infrared mapping spectrometer. Icarus 318, 22–41.
Crown, D., et al., 2018. Geologic mapping of the Urvara and Yalode quadrangles on Ceres. Icarus 316, 167–190.
Dalle Ore, C.M., Protopapa, S., Cook, J., Grundy, W., Cruikshank, D., Verbiscer, A., Ennico, K., Olkin, C., Stern, S., Weaver, H., et al., 2018. Ices on Charon: distribution of H2O and NH3 from New Horizons LEISA observations. Icarus 300, 21–32.
De Sanctis, M., et al., 2012. Spectroscopic characterization of mineralogy and its diversity across vesta. Science 336, 697–700.
De Sanctis, M., Frigeri, A., Ammannito, E., Tosi, F., Marchi, S., Zambon, F., Raymond, C. A., Russell, C.T., 2015. Mineralogy of Marcia, the youngest large crater of Vesta: character and distribution of pyroxenes and hydrated material. Icarus 248, 392–406.
Denevi, B.W., et al., 2012. Pitted terrain on Vesta and implications for the presence of volatiles. Science 338, 246–249. https://doi.org/10.1126/science.1225374.
Dumas, C., Terrile, R.J., Brown, R.H., Schneider, G., Smith, B.A., 2001. Hubble Space Telescope NICMOS spectroscopy of Charon's leading and trailing hemispheres. Astron. J. 121 (2), 1163.
Ermakov, A.I., et al., 2017. Constraints on Ceres' internal structure and evolution from its shape and gravity measured by the Dawn spacecraft. J. Geophys. Res. 123, 2267–2303.
Ferguson, S., Rhoden, A., Ki9rchoff, M., 2020. Small Impact Crater Populations on Saturn's Moon Tethys and Implications for Source Impactors in the System. J. Geophys. Res. 125, e2020JE006400.
Fu, R., Ermakov, E., Marchi, S., Castillo-Rogez, J.C., Raymond, C.A., Hager, B.H., Zuber, M.T., King, S.D., Bland, M.T., De Sanctis, M.C., Preusker, F., Park, R.S., Russell, C.T., 2017. The interior structure of Ceres as revealed by surface topography. Earth Planet Sci. Lett. 476, 153–164.
Greeley, R., Fink, J.H., Gault, D.E., Guest, J.E., 1982. Experimental simulation of impact cratering on Icy satellites. In: Morrison, D. (Ed.), Satellites of Jupiter. Univ. Arizona Press, pp. 340–378.
Grundy, W., Binzel, R., Buratti, B., Cook, J., Cruikshank, D., Dalle Ore, C., Earle, A., Ennico, K., Howett, C., Lunsford, A., 2016. Surface compositions across Pluto and Charon. Science 351 (6279), aad9189.

Hesse, M., Castillo-Rogez, J., 2019. Thermal evolution of the impact-induced cryomagma chamber beneath Occator crater on Ceres. Geophys. Res. Lett. 46, 1213–1221.
Hiesinger, H., et al., 2016. Cratering on Ceres: implications for its crust and evolution. Science 353. https://doi.org/10.1126/science aaf4759.
Hughson, K.H.G., Russell, C.T., Schmidt, B.E., Chilton, H.T., Sizemore, H., Schenk, P.M., Raymond, C.A., 2019a. Fluidized appearing ejecta on Ceres: implications for the mechanical properties, frictional properties, and composition of its shallow subsurface. J. Geophys. Res. 124, 1819–1839. https://doi.org/10.1029/2018JE005666.
Hughson, K.H.G., Russell, C.T., Schmidt, B.E., Travis, B., Preusker, F., Neesemann, A., et al., 2019b. Normal faults on Ceres: insights into the mechanical properties and thermal history of Nar Sulcus. Geophys. Res. Lett. 46, 80–88. https://doi.org/10.1029/2018GL080258.
Keil, K., Stoeffler, D., Love, S.G., Scott, E.R.D., 1997. Constraints on the role of impact heating and melting in asteroids. Meteorit. Planet. Sci. 32, 349–363.
Kenkmann, T., 2002. Folding in seconds. Geology 30, 231–234.
Kenkmann, T., Dalwigk, I., 2000. Radial transpression ridges: a new structural feature of complex impact craters. Met. Planet. Sci. 35, 1189–1201.
Roatsch, T., Kersten, E., Matz, K.-D., Preusker, F., Scholten, F., Elgner, S., Schroeder, S.E., Jaumann, R., Raymond, C.A., Russell, C.T., 2016. DAWN FC2 derived Ceres HAMO DTM SPG V1.0, DAWN-A-FC2-5-CERESHAMODTMSPG-V1.0. In: NASA Planetary Data System. https://sbnarchive.psi.edu/pds3/dawn/fc/DWNCHSPG_2/.
Kirchoff, M.K., Bierhaus, E.B., Dones, L., Robbins, S.J., Singer, K.N., Wagner, R.J., Zahnle, K.J., 2018. In: Schenk, P., Clark, R.N., Howett, C.J.A., Verbiscer, A.J., Waite, J.H. (Eds.), Cratering histories in the saturnian system. In Enceladus and the icy moons of Saturn. University of Arizona Press, Tucson, Arizona, pp. 267–284.
Krohn, K., Jaumann, R., Otto, K., Hoogenboom, T., Wagner, R., Buczkowski, D.L., Garry, B., Williams, D.A., Yingst, R.A., Scully, J., De Sanctis, M.C., Kneissl, T., Schmedemann, N., Kersten, E., Stephan, K., Matz, K.-D., Pieters, C.M., Preusker, F., Roatsch, T., Schenk, P., Russell, C.T., Raymond, C.A., 2014a. Mass movement on Vesta at steep scarps and crater rims. Icarus 244, 120–132. https://doi.org/10.1016/j.icarus.2014.03.013.
Krohn, K., Jaumann, R., Elbeshausen, D., Kneissl, T., Schmedemann, N., Wagner, R., Voigt, J., Otto, K., Matz, K.D., Preusker, F., Roatsch, T., Stephan, K., Raymond, C.A., Russell, C.T., 2014b. Asymmetric craters on Vesta: impact on sloping surfaces. Planet. Space Sci. 103, 36–56. https://doi.org/10.1016/j.pss.2014.04.011.
Krohn, K., Jaumann, R., Wickhusen, K., Otto, K.A., Kersten, E., Stephan, K., Wagner, R.J., Raymond, C.A., Russell, C.T., 2019. Asymmetric craters on the dwarf planet Ceres—results of second extended Mission data analysis. Geosciences 9, 475. https://doi.org/10.3390/geosciences9110475.
Krohn, K., von der Gathen, I., Buczkowski, D.L., Jaumann, R., Wickhusen, K., Schulzeck, F., Stephan, K., Wagner, R., Scully, J.E.C., Raymond, C.A., Russell, C.T., 2020. Fracture geometry and statistics of Ceres' floor fractures. Planet. Space Sci. 187, 104955. https://doi.org/10.1016/j.pss.2020.104955.
Marchi, S., et al., 2012. The violent collisional history of asteroid 4Vesta. Science 336, 690–694.
Marchi, S., Bottle, W., Cohen, B., Wunnemann, K., Kring, D., McSween, H., De Sanctis, M., O'Brien, D., Schenk, P., Raymond, C., Russell, C., 2013. High-velocity collisions from the lunar cataclysm recorded in asteroidal meteorites. Nat. Geosci. 6, 303–307.
Mao, X., McKinnon, W., 2020. Spin evolution of Ceres and Vesta due to impacts. Met. Planet. Sci. 55, 2493–2518.
Melosh, H.J., 1989. Impact Cratering as a Geologic Process. Oxford Univ. Press.
Michalik, K.A., Otto, R., Jaumann, 2020. Geomorphologic Setting of Pitted Terrains on Vesta and Implications for Their Formation. LPSC #1958.
Moore, J.M., et al., 2016. The geology of Pluto and Charon through the eyes of New Horizons. Science 351, 1284–1293. https://doi.org/10.1126/science.aad7055 aad7055.
Nathues, A., 14 others, 2020. Recent cryovolcanic activity at Occator crater on Ceres. Nat. Astronomy 4, 794–801. https://doi.org/10.1038/s41550-020-1146-8.
Neesemann, A., van Gasselt, S., Schmedemann, N., Marchi, S., Walter, S., Preusker, F., Michael, G., Kneissl, T., Hiesinger, H., Jaumann, R., Roatsch, T., Raymond, C., Russell, C., 2019. The various ages of Occator crater, Ceres: Results of a comprehensive synthesis approach. Icarus 320, 60–82. https://doi.org/10.1016/j.icarus.2018.09.006.
Otto, K.A., Jaumann, R., Krohn, K., Matz, K.-D., Preusker, F., Roatsch, T., Schenk, P., Scholten, F., Stephan, K., Raymond, C.A., Russell, C.T., 2013. Mass-wasting features and processes in Vesta's south polar basin Rheasilvia. J. Geophys. Res. 118, 1–16. https://doi.org/10.1002/2013JE004333.
Otto, K.A., Jaumann, R., Krohn, K., Spahn, F., Raymond, C.A., Russell, C.T., 2016. The Coriolis effect on mass wasting during the Rheasilvia impact on asteroid Vesta. Geophys. Res. Lett. 43 https://doi.org/10.1002/2016GL071539.
Otto, K.A., Marchi, S., Trowbridge, A., Melosh, H.J., Sizemore, H.G., 2019. Ceres Crater degradation inferred from concentric fracturing. J. Geophys. Res. 124, 1–16. https://doi.org/10.1029/2018JE005660.
O'Brien, D., Marchi, S., Morbidelli, A., Bottke, W., Schenk, P., Russell, C.T., Raymond, C., 2014. Constraining the cratering chronology of Vesta, Planet. Space Sci. 103, 131–142.
Park, R.S., Buccino, D.R., 2018. Ceres SPC shape model dataset V1.0. DAWN-A-FC2-5-CERESSHAPESPC-V1.0. In: NASA Planetary Data System. https://sbnarchive.psi.edu/pds3/dawn/fc/DWNCSPC_4_01/DATA/.
Pierazzo, E., Vickery, A., Melosh, H.J., 1997. A reevaluation of impact melt production. Icarus 127, 408–423.
Pike, R.J., 1980. Control of crater morphology by gravity and target type: Mars, Earth, Moon. In: Proc. Lunar Planet Sci. Conf., 11th, pp. 2159–2189.
Plescia, J., Cintala, M., 2012. Impact melt in small lunar highland craters. J. Geophys. Res. 117, E00H12.
Prettyman, T.H., Yamashita, N., Toplis, M.J., McSween, H.Y., Schorghofer, N., Marchi, S., Feldman, W.C., Castillo-Rogez, J.C., Forni, O., Lawrence, D.J., Ammannito, E., Ehlmann, B.L., Sizemore, H.G., Joy, S.P., Polanskey, C.A., Rayman, M.D., Raymond, C.A., Russell, C.T., 2017. Extensive water ice within Ceres' aqueously altered regolith: evidence from nuclear spectroscopy. Science 355 (6320), 55–59. https://doi.org/10.1126/science.aah6765.
Preusker, F., Scholten, F., Matz, K.-D., Roatsch, T., Jaumann, R., Raymond, C.A., Russell, C.T., 2016. DAWN FC2 DERIVED VESTA DTM SPG V1.0, DAWN-A-FC2-5-VESTADTMSPG-V1.0. In: NASA Planetary Data System. https://sbn.psi.edu/pds/resource/dawn/dwnvfcshape.html.
Raponi, A., et al., 2018. Variations in the amount of water ice on Ceres' surface suggest a seasonal water cycle. Science Adv. 4, eaao3757.
Robbins, S., et al., 2020. Depths of Pluto's and Charon's craters, and their simple-to-complex transition. Icarus 356, 113902.
Russell, C.T., Raymond, C.A., Coradini, A., McSween, H.Y., Zuber, M.T., Nathues, A., De Sanctis, M.C., Jaumann, R., Konopliv, A.S., Preusker, F., Asmar, S.W., Park, R.S., Gaskell, R., Keller, H.U., Mottola, S., Roatsch, T., Scully, J.E.C., Smith, D.E., Tricarico, P., Toplis, M.J., Christensen, U.R., Feldman, W.C., Lawrence, D.J., McCoy, T.J., Prettyman, T.H., Reedy, R.C., Sykes, M.E., Titus, T.N., 2012. Dawn at Vesta: testing the protoplanetary paradigm. Science 684–686.
Russell, C., Raymond, C.A., Ammannito, E., Buczkowski, D.L., DeSanctis, M.C., Hiesinger, H., Jaumann, R., Konopliv, A.S., McSween, H.Y., Nathues, A., Park, R.S., Pieters, C.M., Prettyman, T.H., McCord, T.B., McFadden, L.A., Mottola, S., Zuber, M.T., Joy, S.P., Polanskey, C., Rayman, M.D., Castillo-Rogez, J.C., Chi, P.J., Combe, J.P., Ermakov, A., Fu, R.R., Hoffmann, M., Jia, Y.D., King, S.D., Lawrence, D.J., Li, J.-Y., Marchi, S., Preusker, F., Roatsch, T., Ruesch, O., Schenk, P., Villarreal, M.N., Yamashita, N., 2016. Dawn arrives at Ceres: exploration of a small, volatile-rich world. Science 353 (6303), 1008–1010. https://doi.org/10.1126/science.aaf4219.
Sarafian, A.R., Nielsen, S.G., Marschall, H.R., Gaetani, G.A., Righter, K., Berger, E.L., 2019. The water and fluorine content of 4 Vesta. Geochim. Cosmochim. Acta 266, 568–581.
Schenk, P.M., 1989. Crater formation and modification on the icy satellites of Uranus & Saturn: depth/diameter & central peak occurrence. J. Geophys. Res. 94, 3812–3832.
Schenk, P.M., 1991. Ganymede and Callisto: complex crater formation and planetary crusts. J. Geophys. Res. 96, 15635–15664.
Schenk, P.M., 1993. Central pit and dome craters: exposing the interiors of Ganymede and Callisto. J. Geophys. Res. 98, 7475–7498.
Schenk, P., 2002. Thickness constraints on the icy shells of the Galilean satellites from a comparison of crater shapes. Nature 417, 419–421.
Schenk, P., Turtle, E., 2009. Europa's impact craters: Probes of the interior. In: Pappalardo, R.T., McKinnon, W.B., Tucson, Khurana K. (Eds.), Europa. University of Arizona Press, Arizona, pp. 181–198.
Schenk, P., et al., 2020a. Impact heat driven volatile redistribution at Occator crater Ceres as a comparative planetary process. Nat. Comm. 11, 3579.
Schenk, P., et al., 2012. The geologically recent giant impact basins at Vesta's south pole. Science 336, 694–697.
Schenk, P., et al., 2018a. Breaking up is hard to do: global cartography and topography of charon from new horizons. Icarus 315, 124–145.
Schenk, P., et al., 2019. The central pit and dome at Cerealia Facula bright deposit & floor deposits in Occator crater, Ceres: Morphology, comparisons & formation. Icarus 320, 159–187.
Schenk, P., Chapman, C., Zahnle, K., Moore, J., 2004. Ages and interiors, the cratering record of the Galilean Satellites. In: Jupiter. Cambridge Press, pp. 427–456.
Schenk, P., Hamilton, D., Johnson, R., McKinnon, W., Schmidt, J., Showalter, M., 2011. Plasma, plumes, & rings: Saturn system dynamics as revealed by global color patterns on its midsize icy satellites. Icarus 211, 740–757.
Schenk, P.and 12 others, 2016. Impact cratering on the small planets ceres and vesta: S-Ctransitions, central pits, and the origin of bright spots. Lunar Planet. Sci. Conf. 47. Abstr. 2697.
Schenk, P., White, O., Bryne, D., Moore, J., 2018b. Saturn's Other Icy Moons: Geologically Complex Worlds in Their Own Right. In: Schenk, P., et al. (Eds.), Enceladus and the Icy Moons of Saturn. Univ. Arizona Press, pp. 237–265.
Schenk, P., Kirchoff, M., Hoogenboom, T., Rivera-Valentín, E., 2020b. The anatomy of fresh complex craters on the mid-sized icy moons of saturn and self-secondary cratering at the Rayed Crater Inktomi (Rhea). Met. Planet. Sci. 55, 2440–2460.
Schmidt, B.E., Hughson, K.H.G., Chilton, H.T., Scully, J.E.C., Platz, T., Nathues, A., Sizemore, H., Bland, M.T., Byrne, S., Marchi, S., O'Brian, D.P., Schorghofer, N., Hiesinger, H., Jaumann, R., Pasckert, J.H., Lawrence, J.D., Castillo-Rogez, J.C., Sykes, M.V., Schenk, P.M., De Sanctis, M.C., Mitri, G., Formisano, M., Li, J.-Y., Reddy, V., LeCorre, L., Russell, C.T., Raymond, C.A., 2017. Geomorphological evidence for ground ice on dwarf planet Ceres. Nat. Geosci. 10, 338–343. https://doi.org/10.1038/ngeo2936.
Schmidt, B.E., Sizemore, H.G., Hughson, K.H.G., et al., 2020. Post-impact cryo-hydrologic formation of small mounds and hills in Ceres's Occator crater. Nat. Geosci. 13, 605–610. https://doi.org/10.1038/s41561-020-0581-6.
Scully, J., et al., 2015. Geomorphological evidence for transient water flow on Vesta. Earth Planet Sci. Lett. 411, 151–163. https://doi.org/10.1016/j.epsl.2014.12.004.
Scully, J.E.C., et al., 2019. Ceres' Occator crater and its faculae explored through geologic mapping. Icarus 320, 7–23.
Scully, J.E.C., et al., 2020a. Can a Short-Lived, Debris-Flow-Like Process Form Curvilinear Gullies, Lobate Deposits and Pitted Terrain on Vesta and Ceres? 51st Lunar and Planetary Science Conference, Abstract #1638.

Scully, J.E.C., et al., 2020b. The varied sources of faculae-forming brines in Ceres' Occator crater emplaced via hydrothermal brine effusion. Nat. Commun. 11, 3680. https://doi.org/10.1038/s41467-020-15973-8.
Senft, L., Stewart, S., 2011. Modeling the morphologic diversity of impact craters on icy satellites. Icarus 214, 67–81.
Singer, K.N., et al., 2019. Impact craters on Pluto and Charon indicate a deficit of small Kuiper belt objects. Science 363 (8), 955–959.
Sizemore, H.G., Platz, T., Schorghofer, N., Prettyman, T.H., De Sanctis, M.C., Crown, D. A., Schmedemann, N., Neesemann, A., Kneissl, T., Marchi, S., Schenk, P.M., Bland, M.T., Schmidt, B.E., Hughson, K.H.G., Tosi, F., Zambon, F., Mest, S.C., Yingst, R.A., Williams, D.A., Russell, C.T., Raymond, C.A., 2017. Pitted terrains on (1) Ceres and implications for shallow subsurface volatile distribution. Geophys. Res. Lett. 44, 6570–6578. https://doi.org/10.1002/2017GL073970.
Sori, M.M., Byrne, S., Bland, M.T., Bramson, A.M., Ermakov, A.I., Hamilton, C.W., Otto, K.A., Ruesch, O., Russell, C.T., 2017. The vanishing cryovolcanoes of Ceres. Geophys. Res. Lett. 44, 1243–1250. https://doi.org/10.1002/2016GL072319.
Vincent, J.-B., Schenk, P., Nathues, A., Sierks, H., Hoffmann, M., Gaskell, R.W., Marchi, S., O'Brien, D.P., Sykes, M., Russell, C.T., Fulchignoni, M., Keller, H.U., Raymond, C., Palmer, E., Preusker, F., 2014. Crater depth-to-diameter distribution and surface properties of (4) vesta. Planet. Space Sci. 103, 57–65.
White, O.L., Schenk, P.M., Dombard, A.J., 2013. Impact basin relaxation on Rhea and Iapetus and relation to past heat flow. Icarus 223, 699–709. https://doi.org/10.1016/j.icarus.2013.01.013.
White, O.L., Schenk, P.M., Bellagamba, A.W., Grimm, A.M., Dombard, A.J., Bray, V.J., 2017. Impact crater relaxation on Dione and Tethys and relation to past heat flow. Icarus 288, 37–52. https://doi.org/10.1016/j.icarus.2017.01.025.
Williams, D., et al., 2014b. The geology of the Marcia quadrangle of asteroid Vesta: assessing the effects of large, young craters. Icarus 244, 74–88.
Williams, D., O'Brien, D., Schenk, P., Denevi, B., Carsenty, U., Marchi, S., Scully, J., Jaumann, R., DeSanctis, M., Ernesto Palomba, H., Ammannito, E., Longobardo, A., Magni, G., Frigeri, A., Russell, C.T., Raymond, C., Davison, T., 2014a. Lobate and flow-like features on asteroid Vesta. Planet. Space. Sci. 103, 24–35.
Yingst, E., et al., 2014. Geologic mapping of Vesta. Planet Space Sci. 103, 2–23.
Zahnle, K., Schenk, P., Levison, H., Dones, L., 2003. Cratering rates in the outer solar system. Icarus 163, 263–289.
Zannoni, M., Hemingway, D., Casajus, L., Tortora, P., 2020. The gravity field and interior structure of Dione. Icarus 345, 113713.
Zeilnhofer, M., Barlow, N., 2020. Latitudinal Variations in Crustal Strength Across Ceres as Revealed by Its Impact Craters. 11th PCC #2023.